THESIS FOR THE DEGREE OF LICENTIATE OF ENGINEERING

Characterization of Solids Mixing in Binary Fluidized Beds

AZKA RIZWANA SIDDIQUI

Department of Space, Earth and Environment

CHALMERS UNIVERSITY OF TECHNOLOGY

Gothenburg, Sweden 2026

Characterization of Solids Mixing in Binary Fluidized Beds

AZKA RIZWANA SIDDIQUI

Department of Space, Earth and Environment
Division of Energy Technology
Chalmers University of Technology
SE-412 96 Gothenburg
Sweden

Printed by Chalmers Reproservice
Chalmers University of Technology
Gothenburg, Sweden 2026

Characterization of Solids Mixing in Binary Fluidized Beds

AZKA RIZWANA SIDDIQUI
Division of Energy Technology
Department of Space, Earth and Environment
Chalmers University of Technology

Abstract

Fluidization is a key technology for handling particulate systems, facilitating enhanced mixing, heat transfer, and mass transfer in gas–solid contact processes. In bubbling fluidized beds used for thermochemical conversion, where multiple solid phases coexist, typically involving a dense bulk solids phase and a dilute lean solids phase, the process performance is strongly governed by the extent of solid–solid mixing. This dependence has driven sustained research efforts focused on understanding the fluid dynamics of bubbling fluidized beds containing heterogeneous solid phases. Much of the existing experimental literature on solids mixing consists of studies under ambient (cold) conditions using the same solids representative of industrial hot applications but fluidized with readily available gases (such as air). This practice neglects the strong influence of temperature-dependent fluid properties on bed hydrodynamics, thereby limiting the validity of such experimental findings. Further, the inability to accurately measure the distribution of solids phases and their flow patterns in a space and time-resolved fashion has constrained the achievement of a mechanistic understanding of mixing in these heterogeneous systems.

This work addresses these gaps by developing a magnetic solids tracing technique for spatiotemporal characterization of axial solids transport and by experimentally evaluating solids mixing under industrially relevant conditions. The study systematically examines the influence on lean solids mixing for varying operating parameters, including fluidization velocity, bed height, lean solids loading, and different types of lean solids undergoing conversion and releasing gas.

The results demonstrate that neglecting the effect of temperature on fluid properties in cold experiments leads to substantial overestimation of bubble size, bed dynamics, and the extent of solids mixing, underscoring the value of fluid-dynamic scaling to capture realistic solids interactions. When hydrodynamic similarity is preserved by accounting for temperature effects, the results indicate that mixing is enhanced with increasing fluidization velocity and bed height, while high lean phase loadings (>10 $\%_{vol}$) promote segregation due to suppressed bubble-driven circulation. Axial transport is dominated by bubble dynamics rather than buoyancy, with mixing of lean solids occurring at lower characteristic frequencies than those associated with bubbles, indicating that not all the bubbles effectively contribute to mixing. The gas release from lean solids introduces an additional transport mechanism. At low fluidization velocities, the gas release modifies the axial distribution of lean solids by generating a localized and transient reduction in solids concentration around the particle, reducing inter-particle interactions between the lean solid particle and the surrounding bulk solids suspension. This reduces the effective drag and friction opposing the particle motion, allowing lean solids to respond differently to their relative density. While at higher fluidization velocities, the gas release from lean solids enhances the lateral dispersion of the particle by up to 40%.

By combining fluid dynamic scaling, novel magnetic tracing technique, and contemplation of effects of gas release from lean solids, this work advances the mechanistic understanding of solids mixing in fluidized beds and delivers novel information about mixing under industrially relevant conditions.

Keywords: Solids mixing, Bed dynamics, Binary fluidized beds, Fluid dynamic scaling, Magnetic solids tracing

List of Publications

This thesis is based on the work presented in the following publications, which are referred to in the text by their Roman numerals:

Paper I Azka Rizwana Siddiqui, Anna Köhler, Diana Carolina Guio Perez, David Pallarès.
The Impact of Fluid-Dynamical Scaling on the Vertical Distribution of Solids in Binary Fluidized Beds
The 25th Edition of The Fluidized Bed Conversion Conference, Nanjing, China, 2025.

Paper II Azka Rizwana Siddiqui, Anna Köhler, Diana Carolina Guio Perez, David Pallarès.
Solids Mixing and Segregation in Binary Fluidized Beds - Defining Spatiotemporal Patterns using a Novel Magnetic Solids Tracing Technique.
Submitted for publication. Under review.

Paper III Azka Rizwana Siddiqui, Jing Shi, Anna Köhler, Diana Carolina Guío-Pérez, David Pallarès.
The Significance of Gas Release on the Mixing of Larger Particles in Bubbling Fluidized Beds.
To be submitted.

Contributions of Authors

Azka Rizwana Siddiqui is the principal author of Papers I–III and was responsible for most of the work, including experimental tasks, data processing, and evaluation. Jing Shi contributed to the majority of the experiments presented in Paper III. Research Specialist Diana Carolina Guío-Pérez contributed to the conceptualization, experimental design, as well as review and discussions across Papers I–III. Professor David Pallarès contributed to the conceptualization, review, and discussions of all three papers. Anna Köhler also made valuable contributions to conceptualization, review, and discussions throughout Papers I–III.

Acknowledgments

My heartfelt gratitude goes to my supervisors, David, Carolina, and Anna, for their constant guidance and support throughout this chaotic journey. I truly tested their patience, yet they continued to guide me with kindness and understanding, helping me find my way forward. I am deeply grateful for their trust and encouragement.

I would also like to extend a big thank you to Rustan. Without his technical expertise, practical support, and generosity with his time, I would not have been able to carry out the laboratory work that formed the foundation of this thesis.

I would also like to thank my colleagues at Energy Technology. Many of us were on the same journey, and sharing it made all the difference. Whether through motivation, thoughtful discussions, or humor during stressful moments, this collective experience kept me going. Farha, Xiaoyun, Nauman, Jing, and Nasrin, you have been an essential part of this journey—thank you.

Special thanks to Sara, who made this foreign country feel like home, offering warmth and friendship when I needed it most.

To my siblings, my unofficial crisis management team, I am profoundly grateful for your presence in my life. Your support is a constant source of strength, and I miss you more with each passing day.

Finally, to my parents, I am endlessly thankful for their love and support.

Yours truly,
Azka Siddiqui

Table of Contents

1 Introduction

1.1 Binary Fluidized Beds

A fluidized bed suspends solid particles in an upward gas flow, creating a dynamic fluid-like state that promotes efficient gas-solid interactions. These interactions enable effective mixing, momentum exchange, and high rates of heat and mass transfer, underpinning extensive use of fluidized beds in industries such as pharmaceuticals, food processing, energy systems, petroleum refining, and mineral processing [1–4]. Among fluidized beds, the simplest and most commonly applied class consists of a single solids phase, often referred to as a unary or monodispersed fluidized bed. These systems have been extensively studied, and their hydrodynamic behavior is relatively well understood. Established models are available to describe flow regimes and particle–fluid interactions [1,2], supporting the reliable design and operation of unary beds. Many industrial applications (e.g., thermochemical conversion, mineral processing, and the food and pharmaceutical industries), however, involve fluidized beds with mixtures of particles that strongly differ in size, density, or shape. These systems, known as binary or multi-component fluidized beds, represent a distinct class of fluidized beds, exhibiting considerably more complex hydrodynamics [5,6].

In a binary fluidized bed, one solids phase is typically present at low concentration and undergoes physical and/or chemical transformation; hereafter referred to as the *lean solids phase*. The second phase, present at higher concentrations, constitutes the bed and is referred to as the *bulk solids phase*. The bulk solids may serve several purposes, such as transferring heat, acting as a catalyst for the reactions, or simply supporting the fluidization of the lean solids phase. Depending on particle properties and operating conditions, the two solid phases may mix to different extents or exhibit segregation and stratification [7–14]. While intensified mixing is generally desirable to ensure effective contact between the solids phases and therefore uniform conversion, uncontrolled segregation is often detrimental to the process, as it can reduce process efficiency and limit operational control. However, a purposeful segregation can sometimes be advantageous in specific contexts, for example, to achieve a narrow residence time distribution or to facilitate particle classification and phase separation [15–17].

Despite extensive research, a detailed understanding of the interactions between these coexisting solid phases in binary fluidized beds remains limited. When the mixing and segregation behavior of lean and bulk solids is properly understood and controlled, binary fluidized beds offer significant opportunities for improved process performance and tailored operations. One such process is the production of biochar in a sand fluidized bed; effective mixing would promote the uniform conversion of biomass into biochar, whereas segregation can be exploited to enable recovery of produced biochar from the sand mixture.

1.2 State of the Art

Mixing and segregation in binary fluidized beds have been extensively studied through a combination of experimental and modeling approaches; however, experimental characterization remains challenging due to the opaque and dynamic nature of gas–solid systems. These challenges are exacerbated under industrially relevant conditions, where high temperatures and large bed dimensions severely limit the applicability of conventional diagnostics. Only a limited number of studies have explored hot, large-scale binary beds, primarily using camera imaging [18,19]. Though these approaches are constrained by limited visibility within the dense bed, leaving much of the bed dynamics largely unresolved.

Owing to the scarcity of measurement techniques suitable for high-temperature applications, most experimental investigations have been conducted under ambient (cold) conditions, allowing the

exploitation of a wider range of diagnostic tools. Direct visual observation [11,20] provides qualitative insights at the surface level but cannot capture the dynamics of the dense bed or quantify solids distribution. Optical imaging [9,21,22] allows tracking of particle motion and bubble activity in real-time, but it is generally restricted to pseudo-2D or near-wall regions, leaving the dense bed principally unobservable. Frozen-bed techniques [8,10,23–28] enable post-mortem spatial analysis but fail to characterize the dynamics of mixing and segregation. Pressure measurements can capture global, time-resolved bed dynamics and bubble activity, yet they do not resolve phase-specific or localized solids behavior.

More advanced diagnostics have been developed to probe the motion within the dense bed. Particle tracking techniques (including radioactive [26,29,30], magnetic [31–33], and positron emission particle tracking [34]) provide detailed Lagrangian information on the trajectories, velocities, and circulation paths of individual tracer particles. While powerful, they typically represent only a small subset of the system and provide limited phase-specific information, even when dummy particles are used [7]. Solids tracing methods, such as including chemical [35,36], thermal [37,38], fluorescent [39,40], radioactive [41], or magnetic [42–47], are designed to quantify the evolution of solid phase concentrations. These techniques provide time-resolved, phase-specific concentration fields but typically yield spatially averaged measurements over the sensing volume, limiting the ability to resolve instantaneous local variations in solids concentration.

Given these experimental limitations, modeling has become an essential tool for studying mixing and segregation in binary fluidized beds. While advanced modeling approaches have advanced considerably, their reliability depends critically on experimental validation, which is not trivial for such complex multiphase systems [48]. As a result, many existing models rely on simplifying assumptions, most commonly based on two-phase theory, in which the bed is represented by bubble and emulsion phases, supplemented by semi-empirical correlations to describe fluid-dynamic behavior and mass conservation to account for the lean solids phase [49]. Computational fluid dynamics (CFD) is also widely employed to model binary fluidized beds through coupled mass and momentum equations that represent the multiphase system using Eulerian-Eulerian and Eulerian-Lagrangian techniques [50,51]. While these approaches can resolve gas–solid interactions in detail, their application to binary systems is limited by the uncertainties in specie-dependent momentum exchange and by the high computational cost associated with fully coupled simulations. As a result, CFD studies of solids mixing are often restricted to simplified geometries, short timescales, or limited operating conditions.

Besides the limitations, several consistent findings have emerged from these experimental and modelling studies. It was shown that the particle properties of the lean and bulk solids—including density, size, and shape—strongly influence mixing and segregation of lean solids [7,11,24]. The particle size and shape interplay with density to affect drag and inertia, influencing the direction and extent of segregation [26]. At the macroscopic scale, mixing in fluidized beds is fundamentally mediated by the bed dynamics, particularly through bubble formation and motion of bulk solids acting as the primary transport mechanism. Bubbles generated by the fluidizing gas, whose growth is influenced by bed height, are the primary drivers of mixing in fluidized beds [52,53] and are commonly referred to as *exogenous bubbles*. These operating conditions, such as superficial gas velocity, bed height, and lean solids loading, can be tuned to promote homogeneous mixing or controlled segregation. Higher gas velocities and taller beds enhance convective mixing but may introduce practical limitations: excessive velocity can cause jetting and gas bypass [28], while excessive height (higher aspect ratio) may induce slugging [54]. The loading of the lean solids phase also affects hydrodynamics; higher loadings increase particle–particle interactions and alter flow patterns, reducing particle mobility and potentially promoting segregation, requiring a balance between the feeding of the lean solids phase and stable

fluidization [34]. A more thorough summary of studies on mixing and segregation is presented in **Paper II** (refer to Table 1). While many consistent findings have been reported, neglecting temperature effects on gas properties (e.g., density and viscosity) in cold experiments leads to Archimedes and Reynolds numbers that are one to two orders of magnitude higher than those representative of industrial hot conditions, thereby violating the fluid-dynamic similarity at these cold conditions and potentially altering the governing gas–solid interaction mechanisms.

In addition to the exogenous bubbles from fluidization gas, bubbles may also form due to gas released from the lean solids phase during conversion processes, giving rise to so-called *endogenous bubbles* [55]. Unlike exogenous bubbles, these endogenously generated bubbles promote the axial segregation of lean solids [56–60] by locally increasing the bed voidage and generating lift forces on the gas-releasing particles [58]. Density differences govern buoyancy, with lighter particles tending to rise and heavier particles to sink [61]. However, gas release from particles can modify the local hydrodynamics, allowing particles to rise or remain suspended even when their density would otherwise promote sinking [58]. It is important to highlight that existing studies on endogenous bubbles have largely been restricted to controlled laboratory conditions, focusing on spherical lean solids uniformly releasing gas over the whole particle surface, injected into a dense bed operated at minimum fluidization velocities. Whilst industrial fluidized beds operate well beyond minimum fluidization velocities, with non-spherical lean solids fed onto the bed surface, the impact of gas-release on mixing of lean solids under such conditions remains unexplored.

As a result, extrapolating the results of present studies to large-scale high-temperature fluidized beds introduces significant uncertainties. This highlights the need for an integrated experimental approach that preserves industrial relevance, employs advanced measurement techniques, and yields fundamental insights into solids mixing.

1.3 Thesis Overview

1.3.1 Aim and Objectives

The aim of this thesis is to investigate solids mixing in binary fluidized beds under industrially relevant conditions, with particular focus on the spatiotemporal characteristics of mixing and on the influence of particle-generated gas release on mixing dynamics.

More specifically, this thesis addresses three key knowledge gaps through the following research questions:

I. What is the impact of neglecting temperature effects on solids mixing?
II. How fast and how deep do lean solids mix in the bed?
III. How does gas release from converting lean solids influence mixing?

To answer these questions and to achieve the stated aim, the following specific objectives are pursued:

1) Develop a measurement technique based on magnetic tracing that enables space and time-resolved acquisition of solid phase concentrations,
2) Evaluate the impact of neglecting temperature-dependent fluid properties on the mixing behavior of lean solids under cold (ambient) conditions,
3) Characterize the extent of solids mixing under transient and steady state operations,
4) Assess the significance of gas release from the lean solids phase on their mixing in a bubbling fluidized bed.

1.3.2 Scope and Outline

This work focuses on the experimental investigation of binary solids in a stationary bubbling fluidized bed, with emphasis on a lean secondary solids phase that is lighter and larger than the Geldart B bulk solids. The study uses both fluid-dynamically scaled cold models and scenarios with a gas-releasing and non-releasing lean solids phase. The analysis covers mixing under steady state conditions as well as transitions under various operating conditions.

Figure 1.1 summarizes the layout of this thesis and the main research questions addressed throughout this work. The thesis is structured around three appended papers, each addressing specific aspects of solids mixing in binary fluidized beds:

1) **Paper I** examines the impact of disregarding the effect of temperature on the axial mixing of the lean solids phase in cold experiments. Deviations in mixing behavior are assessed through axial concentration profiles of the lean solids phase and spectral analysis of concentration fluctuations associated with bubbles.
2) **Paper II** analyses the solids mixing under both steady and transient operating conditions. Characteristic mixing lengths and times associated with the onset of mixing are determined. Steady-state mixing dynamics are interpreted through solids concentration fluctuations and bubble frequencies. A mixing index is used to summarize steady-state mixing behavior across varying operating parameters.
3) **Paper III** explores the significance of gas release on mixing of lean solids under bubbling conditions using probability density functions of axial distributions and dispersion coefficients to quantify the mixing behavior.

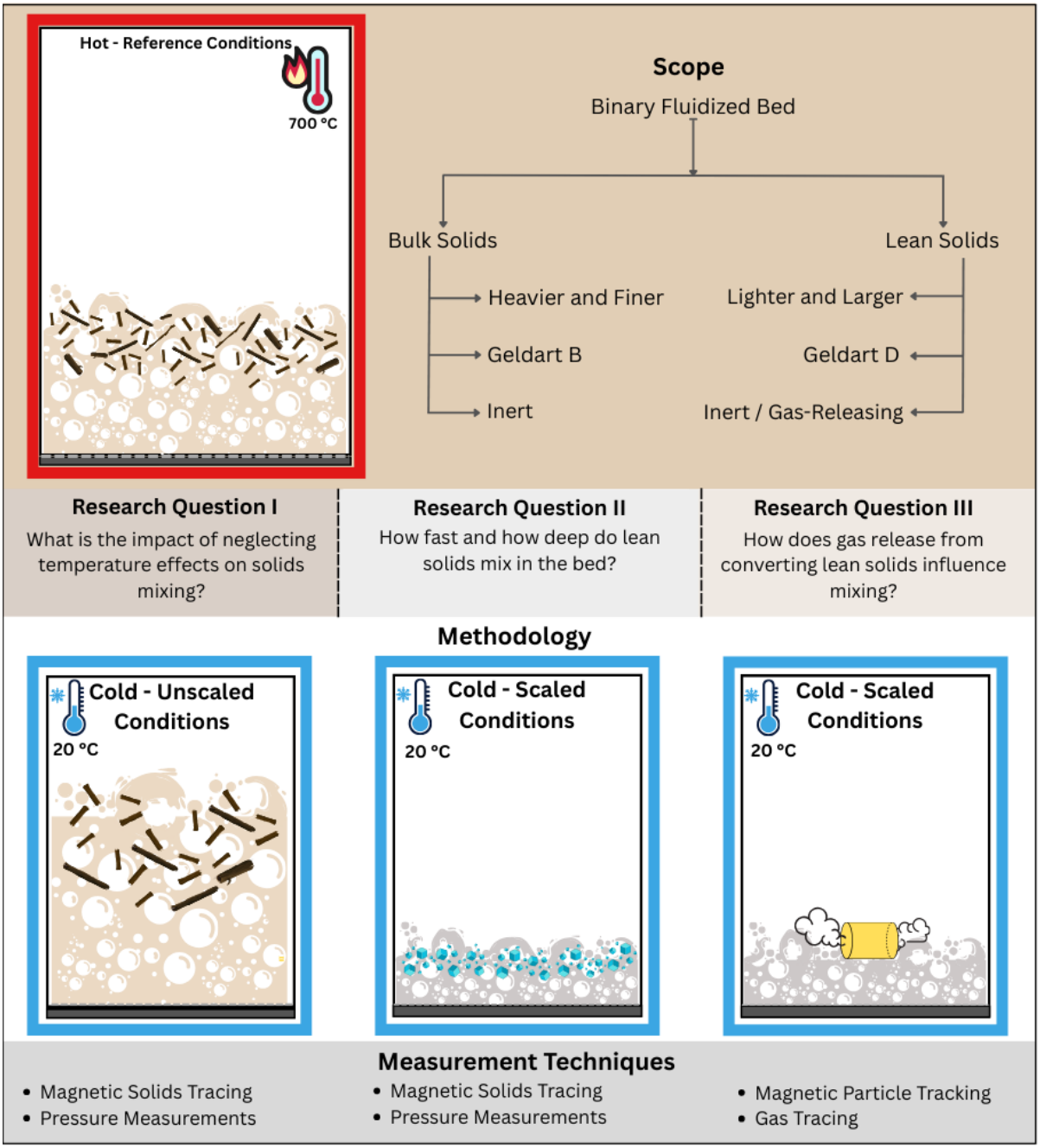

Figure 1.1 Overview of the thesis structure, highlighting the addressed research questions and defined scope.

2 Theory

2.1 The Mixing of Lean Solids

The spatial distribution of the lean solids, their residence time within the dense bed, and their overall mixing dynamics evolve from the interplay between drag-driven circulation of bed solids and particle-specific buoyancy-induced segregation. The drag-driven circulation is governed by the momentum transfer between the lean particles and their surrounding dense suspension, while buoyancy creates an inherent tendency for lighter particles to remain near the dense bed surface, whereas heavier particles preferentially sink into the dense bed.

Bubbles from fluidization gas (often termed as *exogenous bubbles*) are pivotal in establishing solids circulation within the bed. As bubbles rise along preferential paths, they generate coherent circulation cells [62] comprising three characteristic regions: the emulsion, the bubble wake, and the splash zone [63]. Bulk solids are entrained into the wake of rising bubbles and transported upward, while the void left behind by the bubble is continuously refilled by downward-moving emulsion. Bubbles upon reaching the bed surface, erupt and eject bulk solids into the splash zone, redistributing particles laterally before they settle back into the bed. The repeated formation and motion of bubbles along preferred paths, therefore, give rise to a series of circulation cells that govern both axial and lateral solids transport.

Lean solids follow these circulation mechanisms to an extent controlled by their physical properties relative to the bulk solids emulsion. Particles that are lighter and larger than the bulk phase tend to follow the circulation patterns established by the bubble flow within the bulk solids [64]. When captured by a rising bubble, lean solids are entrained into the bubble wake and carried upward through the bed. Conversely, as the emulsion phase moves downward to refill bubble-induced voids, lean solids are dragged into this downward flow, contributing to axial transport within the dense bed, also referred to as axial mixing. In addition to axial motion, the passage of rising bubbles induces oscillations in the surrounding suspension, laterally pushing the lean solids within the dense phase. Upon reaching the bed surface, bubble eruption ejects lean solids into the splash zone, contributing to lateral mixing. **Figure 2.1** illustrates the mechanism of mixing of lean solids in a bubbling fluidized bed.

Overall, axial mixing of the lean solids phase arises from the interlinked upward transport in bubble wakes and downward motion of the dense emulsion, while lateral mixing is primarily driven by bubble eruption and particles splashing at the bed surface. The balance between these mechanisms and their competition with buoyancy-driven segregation ultimately determines the spatial distribution and mixing state of the lean solids phase in bubbling fluidized beds.

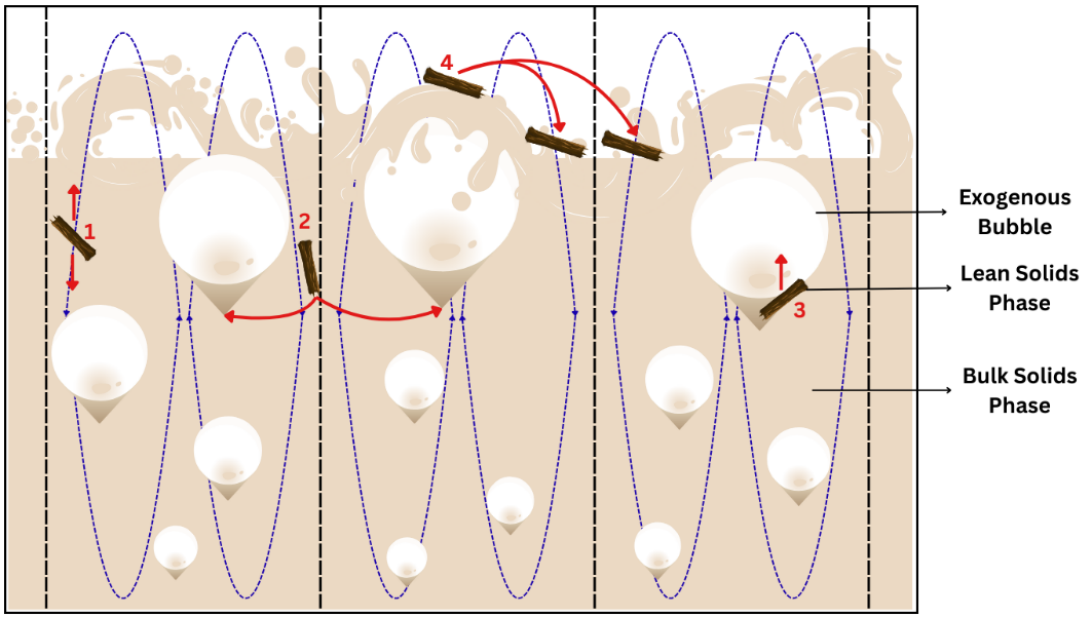

Figure 2.1: Conceptual schematic of the motion of lean solids within a fluidized bed (adapted from [65]**), illustrating particle-specific segregation and circulation-driven mixing mechanisms: (1) transport governed by buoyancy–drag competition within the downward-moving emulsion, (2) entrainment within rising bubbles, (3) upward transport in the bubble wake, and (4) lateral redistribution via splashing upon bubble eruption at the bed surface.**

When the lean solids phase undergoes a conversion that implies a significant release of gas, an additional transport mechanism comes into play that alters the particle motion. It has been shown that, when the particle is immersed in the dense bed, the outward gas flux from the particle surface (*Stefan flow*) locally reduces the surrounding solids concentration, potentially forming a gas pocket (commonly referred to as an *endogenous bubble*) around the particle [56,58–60,66]. This gas pocket generates a lift, partially counteracting the sinking tendency of heavier lean particles while further enhancing the buoyancy of lighter particles [58]. This is the gas release from the particle that modifies the momentum transfer between gas-releasing lean solids and their surrounding suspension and therefore can significantly influence both mixing and segregation behavior within the bed. However, when a gas-releasing particle is located over the bed surface, gas is released directly into the freeboard without forming an endogenous bubble [60]. These two scenarios are illustrated schematically in **Figure 2.2**.

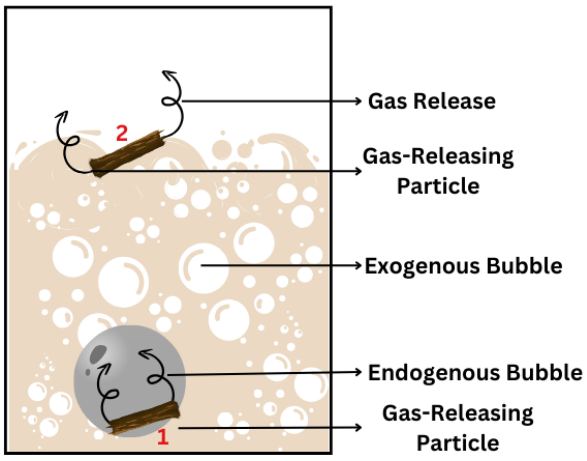

Figure 2.2: Schematic of two gas-releasing fuel particles in a bubbling fluidized bed: particle (1) within the dense bed forming an endogenous bubble, and particle (2) above the bed surface releasing gas directly without forming an endogenous bubble.

2.2 Mathematical Descriptions

In the quantification of fluidized bed dynamics, *bed voidage* (ε_g) – defined as the volume fraction of the bed occupied by gas – and *solids holdup* ($\varepsilon_{s,bulk}$, $\varepsilon_{s,lean}$) – defined as the volume fraction of the bed occupied by solid particles – are fundamental parameters for characterizing the bed. For the binary system, *bed voidage* can be determined from the following relationship:

The volumetric fractions (ε) of the gas phase, bulk solids, and lean solids must sum to unity:

$$\varepsilon_g + \varepsilon_{s,bulk} + \varepsilon_{s,lean} = 1 \quad [2.1]$$

Provided that the *bed density*, (ρ_{bed}), defined as the mass of solid particles per unit volume of the suspension, can be expressed in terms of the volumetric fractions of solids and gas:

$$\rho_{bed} = \rho_{s,bulk}\varepsilon_{s,bulk} + \rho_{s,lean}\varepsilon_{s,lean} + \rho_g\varepsilon_g \quad [2.2]$$

Although the gas contribution is formally included in Eq. 2.2, it is typically very small compared to the solids and can often be neglected. In this case, the bed density is effectively determined by the solids alone, and the axial pressure drop across a bed section is given by:

$$\Delta P = \rho_{bed} g \Delta h \quad [2.3]$$

Pressure fluctuations arise from the complex interactions between the gas and solid phases and therefore contain valuable information about bed hydrodynamics. When analyzed using statistical, spectral analysis, and nonlinear methods, pressure signals can be used to identify different fluidization regimes and characterize bubble dynamics [67]. In particular, the amplitude and temporal structure of pressure fluctuations provide insights into the bed's hydrodynamic behavior, including bubble formation, growth, coalescence, and the extent of solids circulation. Analysis in the time domain alone may not fully capture the complexity of the bed; isolating specific phenomena, such as bubble formation and motion, often requires frequency-domain or spectral analysis.

Frequency-domain analysis addresses this limitation by decomposing the pressure signal into its constituent components, thereby enabling a clearer association between observed fluctuations and the underlying physical mechanisms [68]. To further distinguish between global and local pressure dynamics, separating the pressure signal into coherent and incoherent components can be done. The *Coherent Output Power* (*COP*) corresponds to pressure fluctuations that are correlated across the bed and are associated with large-scale phenomena such as gas compression, distributor effects, and surface bubble eruptions. In contrast, the *Incoherent Output Power* (*IOP*) represents localized pressure fluctuations arising from individual bubble passage and small-scale turbulence [69].

The incoherent component is of particular relevance, as it enables the estimation of a characteristic gas void length related to the bubble diameter [69]. The bubble diameter has been shown to scale with the standard deviation of the IOP signal according to:

$$D_b \sim \frac{\sigma_{IOP}}{\rho_{mix} g (1-\varepsilon_{mf})} \quad [2.4]$$

Where, σ_{IOP} is the standard deviation of the incoherent pressure fluctuations, $\rho_{mix}$is the effective mixture density, g is the gravitational acceleration, and $(1-\varepsilon_{mf})$ is the solids holdup at the minimum fluidization velocity, with ε_{mf} denoting the bed voidage at minimum fluidization.

For a binary particle mixture, the *effective mixture density* (ρ_{mix}) accounts for particle composition and is used to predict both bubble behavior and solids mixing dynamics in fluidized beds, and is calculated based on the densities and volume fractions of the constituent particles [70] :

$$\rho_{mix} = \rho_{s,bulk}(1 - \varkappa_{lean}) + \rho_{s,lean}\varkappa_{lean} \quad [2.5]$$

where $\varkappa_{lean}$ is the volumetric loading of the lean solids phase, defined as the volume fraction of lean solids added relative to the total solids volume in the system, and is given by:

$$\varkappa_{lean} = \frac{\varepsilon_{s,lean}}{\varepsilon_{s,bulk} + \varepsilon_{s,lean}}$$

Additional parameters are used to characterize the distribution and mixing of the lean solid phase. Given an axial distribution of a solid phase, in this work, the extent of axial mixing is evaluated by a *mixing index*, M, which compares the fully mixed and fully segregated states, and is defined as:

$$M = 1 - \frac{\sigma_{mixed}}{\sigma_{segregated}} \quad [2.7]$$

where σ_{mixed} and $\sigma_{\text{segregated}}$ denote the standard deviation of the lean solids concentration in the mixed and segregated states of reference, respectively. Specifically:

- The fully mixed state corresponds to a uniform solids distribution along the bed, where the concentration at each axial position equals the average concentration.
- The fully segregated state represents the opposite extreme, with solids concentrated in one region of the bed and absent elsewhere, yielding the maximum possible variation along the bed.

The mixing index increases with the degree of axial mixing, yielding $M = 0$ for complete segregation and $M = 1$ for perfect mixing, and serves as a global metric for comparing mixing performance across operating conditions.

Lateral mixing is quantified within a Lagrangian framework using an analogy to Brownian motion, assuming stochastic particle motion of the lean solids within a statistically homogeneous suspension of bulk solids. Under this assumption, the *lateral dispersion coefficient* of the lean solids (D_{lean}) is calculated using the Einstein relation for Brownian motion [71]:

$$D_{lean} = \frac{1}{2}\frac{\langle \Delta_{xy} \rangle^2}{\Delta t} \quad [2.8]$$

where Δ_{xy} is the lateral displacement over the time interval Δt, and $\langle \cdot \rangle$ denotes ensemble averaging. To ensure that the calculated dispersion reflects macroscopic mixing rather than local oscillations, small-scale motions are filtered using a threshold value for length, following the methodology of [72].

2.3 Fluid-Dynamic Scaling

Due to the practical and technical challenges associated with conducting experiments in hot, large-scale fluidized beds, laboratory investigations are commonly performed under cold conditions. To ensure that results obtained at laboratory scale can be interpreted as representative of the industrial systems, fluid-dynamic scaling laws are applied.

Fluid-dynamic scaling aims to maintain geometric, kinematic, and dynamic similarity between the laboratory model and the reference industrial system. This is achieved by reformulating the governing continuity and momentum equations in dimensionless form, from which the key dimensionless groups that characterize the gas–solids interactions are identified [73–76]. Glicksman proposed a full set of these dimensionless groups [73], which is adopted in this work:

$$\frac{u_0^2}{gL}, \frac{\rho_s}{\rho_g}, \frac{\rho_s u_0 d_s}{\mu_g}, \frac{\rho_g u_0 L}{\mu_g}, \frac{L}{D}, \frac{G_s}{\rho_s u_0}, \emptyset, PSD \quad [2.9]$$

This set consists of seven dimensionless groups, i.e., Froude number, solid-to-gas density ratio, the particle Reynolds number, the fluid Reynolds number, the bed geometry, the solids circulation flux, the

particle sphericity, and the particle size distribution. In bubbling fluidized beds, G_s is not a relevant control parameter, as particle motion is primarily driven by bubble-induced agitation. Particle sphericity and size distribution are kept constant in this study because nearly spherical, narrowly sized particles are used, minimizing their influence on bed dynamics. By selecting an appropriate combination of gas and solids while preserving these dimensionless groups, one can determine scaling factors for length, time, and mass, providing a systematic way to link the two systems.

In the context of binary fluidized beds, proper scaling is particularly critical, as mixing and segregation are highly sensitive to changes in gas–solids interaction and bubble dynamics. When scaling is correctly applied, essential bed characteristics are preserved, including bed voidage and expansion, bubble size distributions and rise velocities, as well as the structure of solids circulation cells and associated mixing timescales [74]. Preserving these features ensures that the coupling between the lean and bulk solids phases remains representative of the industrial system. By preserving all relevant dimensionless numbers, the simulated system reproduces the hot reference hydrodynamics, while secondary parameters, such as particle size distribution, shape, or mechanical/chemical/thermal properties of both solid phases, are not explicitly accounted for and are not expected to affect the key mixing behavior

The pressure drop across the distributor plate and the bed plays a key role in establishing and maintaining fluidization. Scaled models must reproduce the correct superficial gas velocity relative to the minimum fluidization velocity to ensure realistic bubble formation, solids expansion, and circulation patterns. Deviations in pressure drop can lead to altered flow regimes [77], uneven fluidization, or channeling, which in turn impact segregation and mixing behavior [32].

Neglecting fluid-dynamic scaling, particularly the influence of temperature-dependent gas properties such as density and viscosity, can lead to substantial deviations in bed hydrodynamics [78]. Such deviations may alter bubble behavior, solids circulation, and particle mobility, ultimately resulting in significant errors in predicting mixing and segregation behavior. Consequently, experimental observations obtained under cold unscaled conditions may not reliably translate to industrial-scale, high-temperature operations with the same gas-solids set.

The applicability of fluid-dynamic scaling to binary fluidized beds has been demonstrated in previous work [19], where lateral mixing of fuel particles in a cold, fluid-dynamically scaled laboratory model was directly compared with that in a large-scale hot fluidized bed. The close agreement observed between the two systems confirms the reliability of fluid-dynamic scaling for capturing the essential mixing behavior in binary bed configurations, providing a robust foundation for the experimental approach adopted in this thesis.

3 Methodology

A unified experimental methodology was applied across all measurement campaigns in this work (detailed in **Section 3.1**). The full set of Glicksman scaling laws [73] are employed to preserve the hydrodynamic similarity between ambient (cold) temperature laboratory setups and a high-temperature industrial reference case.

Table 3.1 summarizes the relevant parameters for this unified methodology, while the descriptions below provide additional information about the units referred to in the table:

1. **Simulated hot reactor** (*industrial reference case*)
   - Industrial unit for pyrolysis of biomass operating at 700°C.
   - Consists of a sand bed fluidized by flue gas.
   - The lean solids are biomass, specifically wood chips and/or pellets.
   - Serves as the reference whose hydrodynamic behavior is to be replicated with the lab experiments.
2. **Cold-scaled model** (*fluid-dynamically downscaled experiments*)
   - Ambient-temperature laboratory setup designed according to the Glicksman scaling laws [73].
   - Uses bronze powder as the bulk solids phase and air as the fluidizing gas.
   - The lean solids are artificial particles fabricated to mimic the shape, size, and density of wood chips or pellets at downscaled conditions.
   - Preserves key dimensionless numbers to achieve fluid-dynamic similarity with the hot industrial reference case.
3. **Cold-unscaled model** (*conventional cold experiments*)
   - Ambient-temperature laboratory setup operated without applying fluid-dynamic scaling laws.
   - Uses the same solids as the industrial reference case (sand and biomass) fluidized by air.
   - The lean solids are artificial particles fabricated to mimic the shape, size, and density of wood chips, replicating the biomass.
   - Included to represent conventional cold experiments that do not preserve fluid-dynamic similarity with the hot industrial reference case.

Table 3.1: Relevant parameters for experimental setups used.

Parameter		Hot reactor simulated	Cold-scaled model	Cold-unscaled model
Operational conditions	Temperature [°C]	700	20	20
	Pressure [atm]	1	1	1
	Minimum fluidization velocity [m/s]	0.16	0.082	0.28
Fluidization gas		Flue gas	Air	Air
	Density [kg/m^3]	0.36	1.20	1.20
	Viscosity [N/(m·s)]	4.07e-5	1.83e-5	1.83e-5
Bed material bulk solids		Sand	Bronze	Sand
	Particle density [kg/m^3]	2,600	8,492	2,600
	Mean particle size [mm]	0.789	0.189	0.789
	Sphericity	0.78	1	0.78
Lean solid phase		Biomass	Synthetic tracer	Synthetic tracer
	Particle density [kg/m^3]	300 – 700	1,000 – 2,400	500
	Mean particle size [mm]	10 – 120	3 – 30	30
	Length-to-Diameter Ratio	1.5	1.5	1.5
Dimensionless Numbers	Density ratio	7,163	7,163	2,166
	Archimedes number	2,742	2,049	45,241
	Particle Reynolds number at U_{mf}	1.13	1.02	15.38
Scaling factors $\left[\frac{\text{cold}}{\text{hot}}\right]$	Length		0.26	--
	Time		0.509	--
	Mass		0.06	--

3.1 Experimental Setup

This work investigates solids mixing in binary fluidized beds through a sequence of three experimental campaigns, each addressing a distinct aspect of the problem. Together, the campaigns move from assessing experimental validity to quantifying mixing behavior, and finally to isolating the effect of particle-generated gas release. All experiments were conducted in stationary cold bubbling fluidized beds, using two laboratory units with cross-sectional areas of 0.30×0.30 m^2 and 0.17×0.17 m^2. An overview of the experimental conditions, measurement techniques, and operating ranges for all three campaigns is provided in **Table 3.2**.

Table 3.2: Overview of experimental campaigns.

Campaign	Methodology	Variables studied (Upscaled)	Focus	Measurement Technique	Lean Solids Phase
I	Comparison of cold, unscaled, and fluid-dynamically downscaled experiments.	1. H_{bed}: 0.30 m 2. $\varkappa_{lean}$: 10 $\%_{vol}$ 3. u_0: $1.5u_{mf} - 3u_{mf}$	Assessment of error between the hot-reference and the unscaled systems	1. Differential Pressure Measurement 2. Magnetic Solids Tracing	Synthetic expanded foam doped with magnetic powder
II	Parametric variation of operating conditions under fluid-dynamically downscaled conditions	1. H_{bed}: 0.15 – 0.46 m 2. H_{bed}/D: 0.13 – 0.4 3. $\varkappa_{lean}$: 3 – 20 $\%_{vol}$ 4. u_0: $1.5u_{mf} - 4u_{mf}$	Description of mixing under representative conditions	1. Differential Pressure Measurement 2. Magnetic Solids Tracing	Synthetic expanded foam doped with magnetic powder
III	Fluid-dynamically downscaled experiments, comparing gas-releasing lean solids with blank controls.	1. Lean solids type: Lighter, Lighter and Larger, Heavier 2. u_0: $1.5u_{mf} - 5u_{mf}$	Effect of gas release on mixing under relevant conditions	1. Magnetic particle tracking 2. Gas tracing	Cylinders with porous caps filled with dry ice and a magnet in the core

Campaign I establishes the extent to which conventional cold experiments can meaningfully represent industrial hot operations, addressing **Research Question I**. Solids mixing in an unscaled cold bed is compared to that in a fluid-dynamically scaled cold model. The latter are first translated to hot-reference conditions using the scaling factors in **Table 3.1**. The comparison focuses on deviations in the mixing behavior of lean solids under otherwise comparable operating conditions. Experiments were conducted in the 0.30 × 0.30 m² unit with different distributor plates: the scaled bronze–air bed used a 2.2 mm perforated plate, while the unscaled sand–air bed used a 3.2 mm plate. These designs ensured that the pressure-drop ratios between distributor and bed were maintained within ±30 % across the two systems.

Campaign II investigates how lean solids mix under industrially relevant conditions, addressing **Research Question II**. Experiments were conducted in the 0.30 × 0.30 m² unit using the scaled bronze–air system. To interpret the results in the context of industrial operation, the cold-scaled data were translated to hot-reference conditions using the scaling factors in **Table 3.1**. Both special and temporal characterization of lean solids mixing is performed. This campaign determines characteristic mixing lengths, mixing times, and dominant temporal scales under both steady and transient operation.

Campaign III isolates a mechanism absent in inert systems: gas release from the lean solids phase, addressing **Research Question III**. A 0.17 × 0.17 m² unit was used to track gas-releasing particles representing converting biomass during drying and devolatilization. This campaign examines how particle-generated gas affects both vertical and lateral mixing of lean solids.

Figure 3.1 illustrates the experimental setups and fabricated tracers used for each experimental campaign.

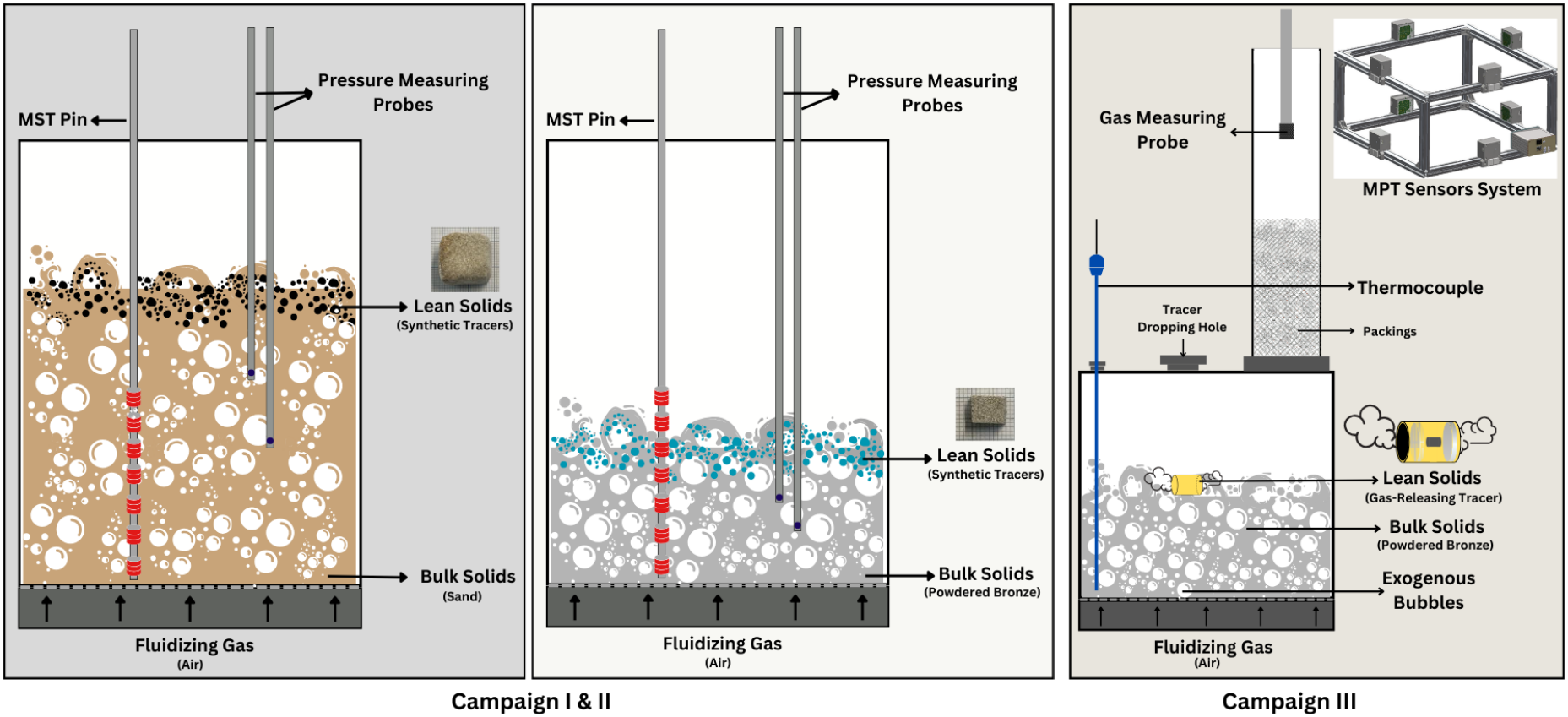

Figure 3.1: Schematics of the cold model setups used in different experimental campaigns.

3.2 Measurement Techniques

3.2.1 Development of Novel Magnetic Solids Tracing Technique

Magnetic solids tracing (MST) is a measurement technique used to trace the spatial and temporal distribution of solids in fluidized beds by exploiting the magnetic properties of tracer particles. In this approach, one solid phase, or a fraction of it, holds ferromagnetic properties [42]. Induction coils placed in or around the bed change their electrical impedance as magnetizable particles pass through the sensing volume (volume of the magnetic field created by the coil). This excitation is converted into an electric signal that is proportional to the concentration of magnetic material. Appropriate calibration is required once the coil and tracer are selected. MST provides high temporal resolution (typically tens to hundreds of hertz), enabling real-time observation of dynamic solid behavior. Previous implementations used large coils to measure spatially averaged concentrations, providing a signal integrated over the entire detection volume. These systems were designed to extract global metrics, such as residence time distributions and solids velocities [43,45–47,79,80].

To yield spatial resolution, a new implementation of the MST technique in the form of a pin-probe configuration has been developed in the present work. The probe consists of a slender rod (1 cm o.d.) equipped with seven miniature induction coils distributed vertically along its length (**Figure 3.2**). The discrete axial placement of the coils enables spatially resolved concentration measurements along the bed height when inserted. Each coil operates at a sampling frequency of up to 100 Hz and is sensitive to magnetically tagged particles within a radial distance of approximately 2 cm from the probe center, providing local yet representative characterization of the surrounding mixture.

Each coil was calibrated to obtain a relationship between electrical impedance response and solids concentration. The calibration was performed using mixtures of magnetic powder and bronze powder with varying volumetric fractions (creating a homogeneous solids mixture). The powders have similar particle size and density, ensuring uniform fluidization behavior. Mixtures of known composition were homogenized by fluidization. Then, with the bed at rest, the impedance response of each coil was measured and correlated with the magnetic tracer fraction. The expected linear dependence was confirmed, and reliable correlations for each of the coils were determined. **Figure 3.2** shows the calibration curve determined and used in this study for experimental **Campaigns I** and **II** (**Table 3.2**).

By collecting signals from the vertically distributed coils, the pin-probe allows reconstruction of spatiotemporal solid concentration fields, making it able to capture both steady-state distributions and transient mixing behavior. The technique enables direct measurement of the local concentration of one solid phase in unary or binary systems. In this study, the method is applied to quantify the distribution of the lean solids phase.

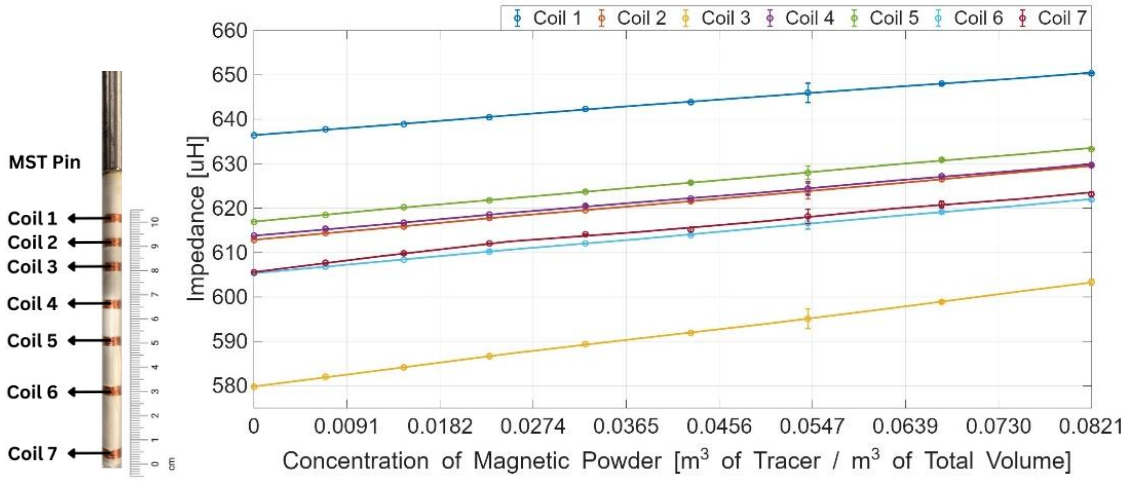

Figure 3.2: Calibration curves for the seven magnetic solid tracing coils embedded in the probe pin.

3.2.2 Experimental Implementation

1) Magnetic Solids Tracing (MST) – **Campaigns I and II**

In **Campaigns I** and **II**, the axial distribution of lean solids was resolved using a pin-probe MST technique with 100 Hz sampling (**Section 3.2.1**). By moving the pin along the bed height, the method captured both mixing and segregation behavior throughout the bed and splash zone. Calibration curves obtained from pure magnetic powder (**Figure 3.2**) were scaled based on the known composition of each fabricated tracer, enabling accurate conversion to lean solids concentration. This measurement technique provided spatiotemporally resolved concentration data, forming the foundation for linking solids motion with bed hydrodynamics.

2) Pressure Measurements – **Campaigns I and II**

To complement MST, time-resolved pressure measurements were collected at ½ and ¾ of the static bed height, as well as in the windbox, also at 100 Hz. These measurements captured pressure fluctuations, overall pressure drop, and bubble activity, offering insight into the hydrodynamic events driving solids motion. Combining MST and pressure data allowed a direct correlation between bubble dynamics and axial solids transport, establishing a clear link between bed hydrodynamics and particle mixing.

3) Magnetic Particle Tracking (MPT) coupled with Gas Tracing – **Campaign III**

Campaign III employed a custom tracer particle designed to mimic both the physical and gas-release behavior of a lean solids particle, tracked using magnetic particle tracking (MPT) [33]. The tracer had a cylindrical shell with porous end caps filled with dry ice to simulate gas evolution during biomass drying and devolatilization. A small permanent magnet (3 × 3 mm) embedded in the tracer enabled real-time 3D tracking of particle motion at 100 Hz using MPT. Particle motion data were synchronized with downstream gas measurements at 1 Hz, allowing direct correlation between gas release and particle movement. A non-releasing blank tracer was also tested to isolate the effect of particle-generated gas on mixing. This approach captured the behavior of lean solids undergoing conversion (releasing gas), providing a more complete understanding of solids mixing (see **Paper III** for details on mimicked gas release rates).

4 Results and Discussion

This chapter presents the main findings of the thesis; selected results address the research objectives outlined in **Section 1.3.1**. **Section 4.1** evaluates the performance of the novel measurement technique developed to measure local solids concentration online, while **Section 4.2** examines the limitations of conventional experimental approaches in resolving local solids concentration and mixing dynamics. **Section 4.3** analyzes the spatiotemporal mixing patterns of the lean solids phase, and **Section 4.4** investigates the effect of gas release on mixing behavior.

Results from cold-unscaled tests are presented as obtained, whereas results from cold-scaled tests are converted to the hot-reference conditions using the scaling factors provided in **Table 3.1**.

4.1 Evaluation of MST Pin-Probe Measurements

The measurements performed with the MST pin-probe and presented here are evaluated in terms of repeatability, accuracy, and representativeness using data from experimental **Campaign II**.

Figure 4.1 shows the time-averaged axial distributions of the lean solids phase, as measured by MST pin-probe, for a bed of H/D = 0.27 with 10%$_{vol}$ loading, and for different fluidization velocities. At low fluidization velocities, the lighter, larger lean solids tend to accumulate near the bed surface [8,26,28]. As velocity increases, particles penetrate deeper and enter the splash zone, broadening the axial distribution toward a more axially uniform profile. This effect is attributed to larger and more frequent bubbles, which enhance bulk solids circulation, which in turn more intensively drags and mixes the lean phase[63,65].

The MST pin-probe also clearly identifies key system features. These include the dense bed height and the transition to the splash zone. The concentration peak aligns closely with the independently measured bed expansion (**Paper II**, Figure 3).

Beyond capturing physically meaningful trends, **Figure 4.1** also demonstrates the robustness of the MST pin-probe technique. The high repeatability of such measurement is reflected in the standard deviation (horizontal bars) across three independent 3-minute repetitions.

Overall, the results show that the MST pin-probe provides representative and repeatable measurements of the lean solids distribution under the tested conditions. The method is responsive under a wide range of concentrations, irrespective of the mixing conditions. The accuracy of the method is further discussed below.

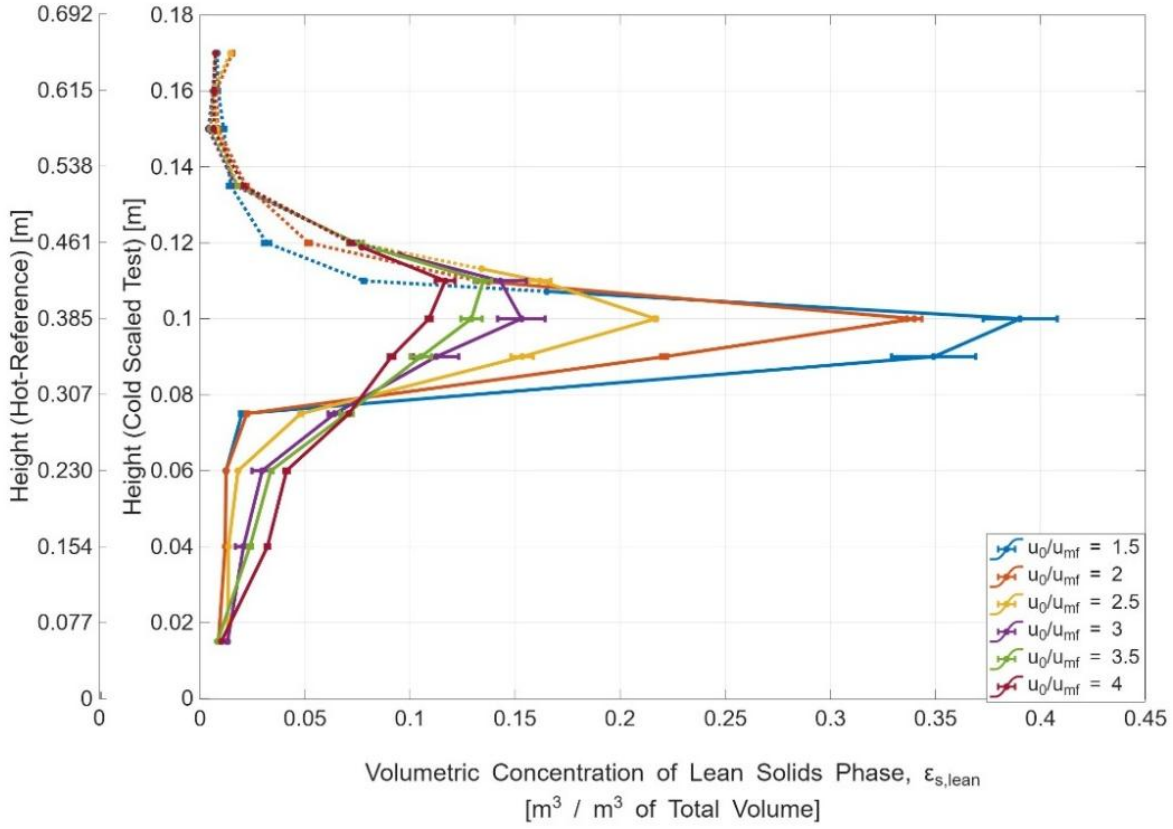

Figure 4.1: Axial distribution profiles of the lean solids phase for different fluidization numbers. Conditions: H/D = 0.27, $\varkappa_{lean}$ = 10%$_{vol}$. Source: Paper II

Mass conservation was evaluated by integrating the lean solids concentration profiles over the full bed height. **Table 4.1** summarizes the reconstructed masses across all operating conditions, which include six fluidization numbers (u_0/u_{mf} = 1.5 – 4), four loadings of lean solids ($\varkappa_{lean}$ = 3 – 20 $\%_{vol}$), and three bed heights (H_{bed} = 0.15 – 0.46 m). Overall, the reconstructed masses agree well with the loaded mass for most cases, as depicted in **Table 4.1**. This confirms that the MST pin satisfactorily provides precise and reliable quantification of the lean solids distribution. Larger deviations occur only at very low or high velocities and loadings, likely due to cross-sectional maldistribution, incomplete axial resolution (e.g., in the splash zone), or strong signal fluctuations.

Table 4.1: Percentages of the mass of the lean solids phase estimated through concentration measurements by MST pin, as compared with the loaded mass. Source: Paper II

Loading of the lean solids phase $\varkappa_{lean}$ [$\%_{Vol}$]	**Aspect ratio H/D [-]**	**Bed height H_{bed} [m]**	**Mass of the lean solids phase m_{lean} [kg]**	**Fluidization Number $\left(\frac{u_0}{u_{mf}}\right)$ [-]**					
				1.5	2	2.5	3	3.5	4
				Ratio of detected lean solids phase with respect to loaded lean solids mass, [%]					
3	0.27	0.3	~6	156 ± 2.92	153.7 ± 2.16	147 ± 3.33	150 ± 2.91	154.5 ± 4.33	146.7 ± 2.75
5	0.27	0.3	~10.4	146.6 ± 2.8	135 ± 2.4	117.2 ± 1.34	108 ± 3.2	108.8 ± 1.91	116.8 ± 2.6
10	0.13	0.15	~10.4	107.8 ± 2.3	102.6 ± 3.0	92.8 ± 1.7	93.9 ± 1.3	91.8 ± 2.0	89.7 ± 3.5
	0.27	0.3	~21	112.4 ± 3.5	104.3 ± 0.6	90.6 ± 1.1	88.8 ± 1.4	86.6 ± 2.2	85.8 ± 1.2
	0.4	0.46	~32	118.3 ± 5.6	102.7 ± 3.4	97.5 ± 4.1	93.0 ± 4.7	92.6 ± 3.6	91.0 ± 3.3
20	0.27	0.3	~48.7	95.35 ± 1.0	94.2 ± 0.36	82.5 ± 0.85	74 ± 0.24	71.4 ± 1.05	71.4 ± 1.45

4.2 Limitations of Cold-Unscaled Test

This section addresses **Research Question I** by examining whether cold-unscaled experiments can reliably represent mixing behavior under hot industrial conditions.

The analysis uses results from experimental **Campaign I**, comparing a fluid-dynamically scaled cold system with a cold-unscaled system. In the scaled configuration, key dimensionless groups are preserved, allowing cold measurements to be translated to hot-reference conditions using the scaling factors in **Table 3.1**. In contrast, the unscaled system does not satisfy dynamic similarity and its results are used as obtained.

All experiments were conducted at a static bed height of H_{bed} = 0.3 m and a lean solids loading of $\varkappa_{lean}$ = 10 $\%_{vol}$. The comparison focuses on three aspects: axial concentration profiles of the lean solids phase; bed dynamics inferred from pressure and concentration fluctuations; and characteristic length scales. The ability of unscaled laboratory tests to realistically represent hot-bed mixing is systematically assessed by contrasting the hot-reference behavior inferred from the scaled configuration with the measured response of the unscaled system.

4.2.1 Axial Profiles of Lean Solids

Figure 4.2 compares the axial distribution of the lean solids phase for the hot-reference case—obtained by translating the cold-scaled measurements using scaling factors listed in **Table 3.1**—with the directly measured cold-unscaled results.

At low fluidization velocities (u_0/u_{mf} = 1.5), both systems exhibit pronounced segregation toward the bed surface (i.e., increased concentration near the surface and lower towards the dense region). This behavior is expected given that the lean solids have lower density and larger size compared to the bulk solids phase. However, the cold-unscaled bed shows a sharper surface peak and a narrower distribution, indicating stronger segregation than predicted for the hot-reference case. Despite this pronounced surface accumulation, measurable concentrations of lean solids remain within the dense region under unscaled conditions. This suggests that some degree of axial transport persists even at this low velocity.

With increasing fluidization velocity, the distributions broaden in both systems, demonstrating enhanced axial transport [61,64,81]. In the hot-reference case, the redistribution remains incomplete. This is, the lean solids penetrate deeper into the dense bed and extend into the splash zone, but a substantial concentration persists near the surface. In contrast, the cold-unscaled bed approaches an almost flat distribution at higher velocities, indicating near-complete axial homogenization.

Overall, the probability density functions reveal a systematic divergence between the two configurations. The unscaled system exaggerates segregation at low velocity and promotes excessive homogenization at higher velocities as compared to the fluid-dynamically scaled version of the experiments.

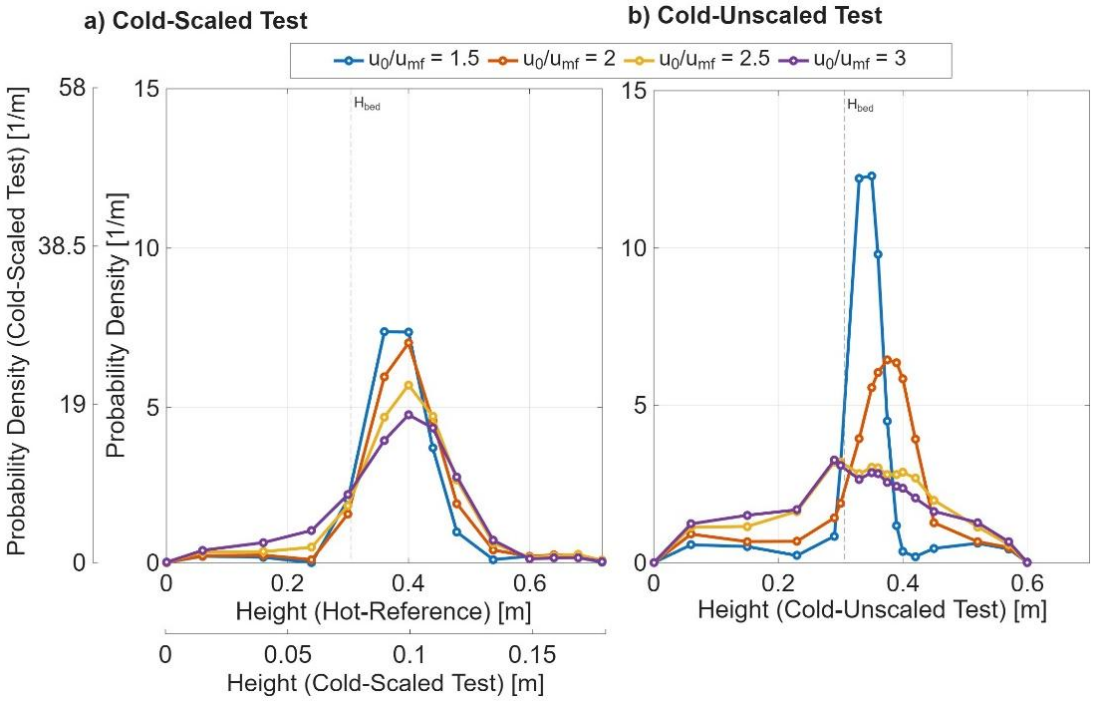

Figure 4.2: Probability density distributions of the lean solids phase concentrations for cold: a) scaled test, b) unscaled test. Dash-line indicates the static bed height. Conditions: H_{bed} = 0.3 m, $\varkappa_{lean}$ = 10%$_{vol}$.

Figure 4.3 quantifies the axial distributions shown in **Figure 4.2** using the mixing index (**Eq. 2.6**). For both systems, the mixing index increases with fluidization velocity [28,82], consistent with enhanced solids circulation [65]. Thus, axial mixing improves as the gas velocity increases in both configurations. Despite this common trend, the magnitude of mixing differs substantially. In the hot-reference case, the mixing index reaches values of approximately 0.7 at higher velocities. These values indicate improved, but still incomplete, axial mixing. In contrast, the cold-unscaled bed approaches values near 0.9. Such values correspond to an almost uniform axial distribution.

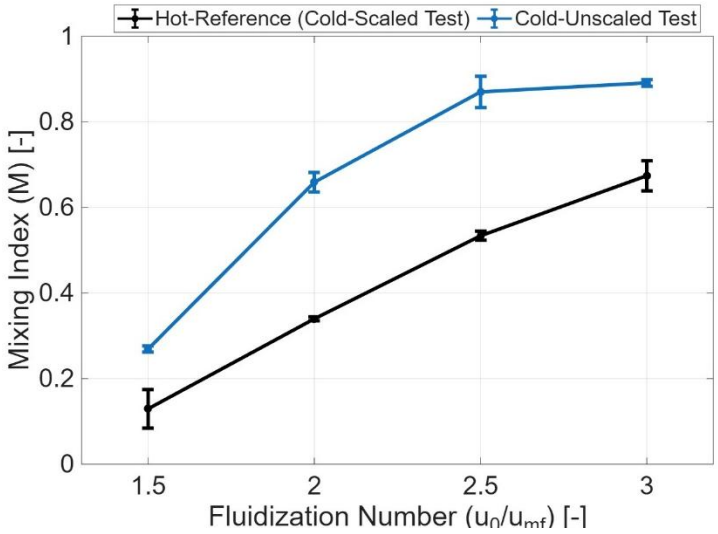

Figure 4.3: Mixing index as a function of fluidization velocity. Conditions: H_{bed} = 0.3 m, $\varkappa_{lean}$ = 10%$_{vol}$.

4.2.2 Bed Dynamics

To explain the divergence in axial lean solids distributions shown in **Figure 4.2**, the underlying bed hydrodynamics is examined. The axial profiles describe the spatial outcome of mixing, whereas the pressure fluctuations reflect the dynamic mechanisms—primarily bubble-induced bed oscillations—that govern solids transport.

Figure 4.4 presents a time series of pressure fluctuations measured at ½ of the static bed height for a bed height of 0.3 m and a lean solids loading of 10 $\%_{vol}$. **Figure 4.4a** corresponds to the hot-reference case inferred from dynamically scaled experiments, while **Figure 4.4b** shows the directly measured response of the cold-unscaled bed.

In both systems, increasing fluidization velocity increases the amplitude of pressure fluctuations, consistent with the intensified bubbling and the enhanced mass oscillations associated with bubble formation, coalescence, eruption, and gas turbulence [67]. Thus, for both configurations, higher excess velocity leads to stronger overall hydrodynamic activity.

However, the magnitude of the fluctuations differs substantially. The cold-unscaled bed exhibits significantly larger pressure amplitudes than the hot-reference case. Since pressure fluctuations are directly linked to bubble growth and eruption dynamics, this indicates that the unscaled system operates with larger hydrodynamic structures and stronger oscillations. This is, the cold-unscaled system exhibits a more vigorous fluidization regime, in which enhanced bubble coalescence and increased flow heterogeneity may occur. Under these conditions, localized channeling and transient gas throughflow are more likely, contributing to a less uniform gas–solid structure compared to the dynamically scaled hot-reference configuration [68], which is likely to promote increased solids redistribution (**Figure 4.2**).

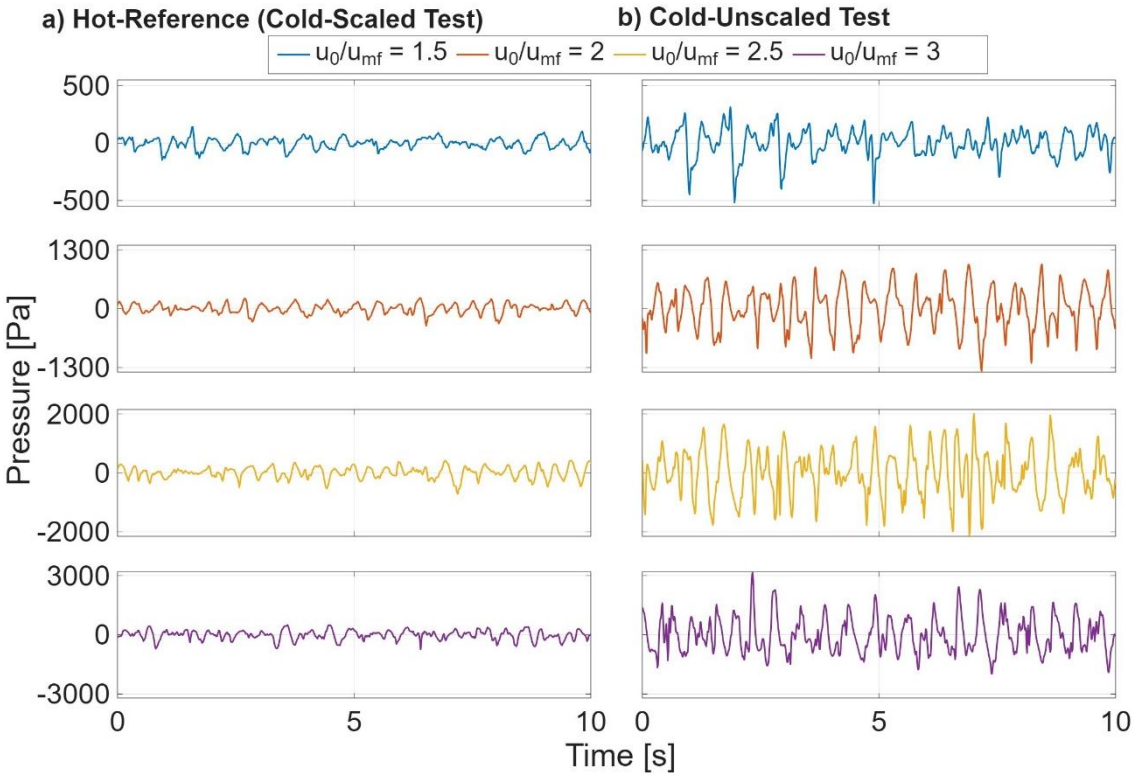

Figure 4.4: Time series of pressure fluctuations measured at the center of the bed for different fluidization velocities: (a) hot-reference conditions obtained by scaling the cold scaled test, and (b) cold unscaled test. Conditions: H_{bed} = 0.3m, and $\varkappa_{lean}$ = 10%$_{vol}$.

To complement the time-domain observation, the characteristic timescales of the mixing event are considered. **Figure 4.5** further examines the dynamic differences between the hot-reference (scaled) and cold-unscaled systems by comparing their normalized cumulative frequency spectra of lean solids concentration and pressure fluctuations.

Figure 4.5a shows the frequency distribution of lean solids concentration fluctuations. In the hot-reference system, median frequencies (f_{50}) remain below 1 Hz and are largely insensitive to fluidization velocity. In contrast, the cold-unscaled system exhibits higher median frequencies ($f_{50} \approx 2$ Hz), with a slight increase as fluidization velocity increases. This indicates more frequent concentration fluctuations under unscaled cold conditions.

Figure 4.5b presents the corresponding pressure spectra, which reflect bubble-driven bed dynamics. Both systems display similar spectral shapes and median frequencies (f_{50} slightly below 3 Hz), showing that the characteristic timescales of bubble formation and eruption are broadly comparable. However, as observed in **Figure 4.4**, the amplitude of these fluctuations is substantially larger in the cold-unscaled bed.

Considering concentration and pressure spectra together reveals an important distinction. Although bubble frequencies are similar, concentration fluctuations occur more often in the cold-unscaled system, suggesting that a larger fraction of hydrodynamic events contributes to measurable lean solids motion. In other words, bubble activity appears more effectively coupled to solids redistribution under unscaled conditions. This stronger coupling is consistent with the enhanced axial mixing observed in **Figure 4.2** and supports the conclusion that cold-unscaled experiments tend to overpredict mixing relative to dynamically scaled hot-reference conditions.

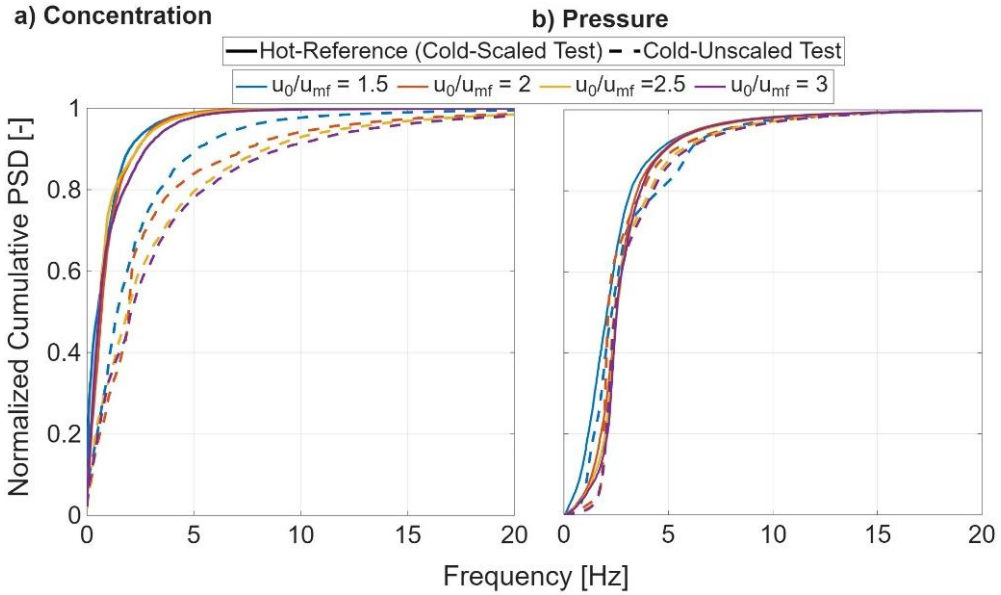

Figure 4.5: Cumulative power spectra of the time series of the a) Concentration and b) Pressure for varying fluidization velocity. Solid lines indicate hot-reference conditions, while dashed lines indicate cold-unscaled test. Conditions: H_{bed} = 0.3m, and $\varkappa_{lean}$ = 10%$_{vol}$.

Figure 4.6 compares bed expansion and characteristic bubble lengths as a function of fluidization velocity for the cold-unscaled and scaled systems (translated to hot-reference conditions). The bed voidage, calculated using **Eqs. 2.1–2.3**, and presented in Figure 4.6a, increases with fluidization velocity in both systems, consistent with literature trends [83–85]. The presence of a secondary solids phase disrupts the dense emulsion packing, increasing gas holdup [86]. This increased gas holdup is particularly pronounced in the cold-unscaled sand bed, where the higher concentration of lean solids in

the dense region (**Figure 4.2**) leads to elevated bed voidage. It should also be noted that voidage measured under cold conditions differs fundamentally from that in a hot, reacting bed. In pyrolyzing or thermochemically converting systems, gas released during devolatilization and char conversion locally increases the gas fraction, an effect that cannot be reproduced in cold experiments. Consequently, absolute voidage values from cold experiments may deviate from those in hot industrial beds [87], underscoring the limitations of cold experiments and possible deviations.

Figure 4.6b shows characteristic lengths of gas voids, calculated using **Eq. 2.4**, as a function of fluidization velocity. At high velocities, i.e., $u_0/u_{mf} = 3$, characteristic lengths of gas voids in the cold-unscaled bed reach approximately 0.024 m, while hot-reference beds exhibit smaller lengths around 0.012 m. These lengths are derived from the standard deviation of Incoherent Output Power (σ_{IOP}), which scales with pressure amplitude and bubble diameter [69]. Since bubble size is inferred indirectly from pressure signals, the method tends to underestimate absolute diameters, particularly for large bubbles where pressure signals may saturate or lose spatial resolution. However, empirical correlations based on excess fluidization velocity enable conversion of the pressure-derived characteristic lengths to actual bubble diameters [86].

The observed differences in bubble size are connected to variations in bed composition, solids-to-gas density ratio, and geometry [87]. The cold-unscaled bed has a lower density ratio (**Table 3.1**), which increases local voidage and promotes bubble coalescence, resulting in larger bubbles. Hot-reference beds, with higher density ratios (**Table 3.1**), suppress excessive coalescence and favor smaller, more uniform bubbles. The presence of lean solids also promotes bubble growth by reducing voids in the dense phase, allowing more gas to accumulate. In the cold-unscaled bed, stronger mixing (**Figure 4.2**) and greater lean solids content may have contributed to larger characteristic lengths of gas voids than in the hot-reference case. Additionally, the relatively tall shape of the cold-unscaled bed (H/D = 1) may favor axial bubble coalescence, resulting in longer, more elongated bubbles and slugs [87], whereas the hot-reference bed with its lower aspect ratio (H/D = 0.27), promotes rather smaller, well-distributed bubbles.

Overall, despite underestimating absolute sizes, the pressure-derived characteristic lengths reliably capture trends in bubble growth and differences between unscaled and dynamically scaled beds and can be quantitatively corrected to actual bubble diameters.

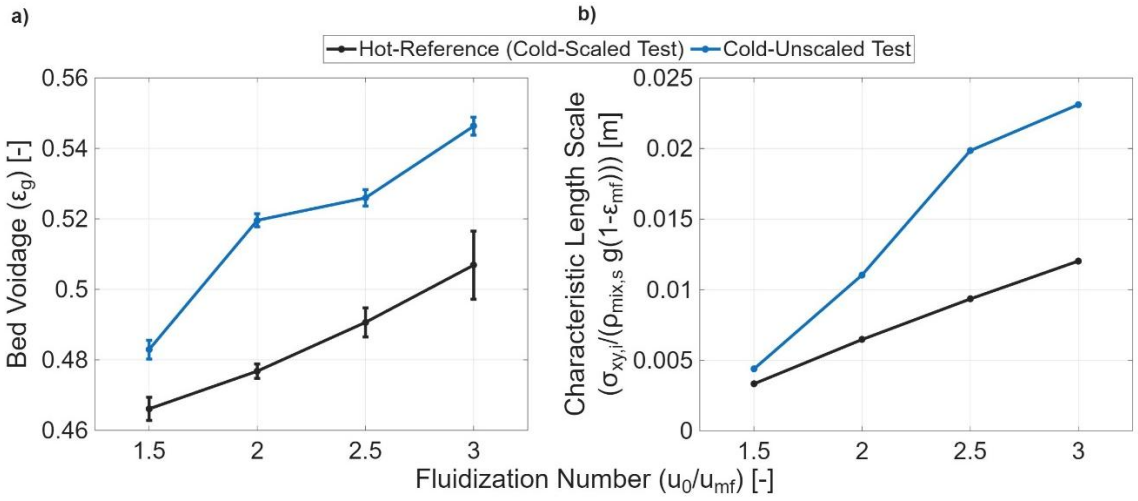

Figure 4.6: a) Time-averaged bed voidage, b) Characteristic length scale of gas voids, as a function of the fluidization velocity. Conditions: H_{bed} = 0.3m, and $\varkappa_{lean}$ = 10%$_{vol}$.

4.3 Spatiotemporal Mixing Patterns

This section presents the results from experimental **Campaign II**, addressing **Research Question I** identified in **Section 1.3.1**. The parametric study varied fluidization velocity (u_0/u_{mf} = 1.5 – 4), lean solids loading ($\varkappa_{lean}$ = 3 – 20%$_{vol}$), and static bed height (H_{bed} = 0.15 – 0.46 m). Here, only selected results are shown, while the complete dataset and analysis are provided in Appended **Paper II**. As summarized in **Table 3.2**, the analysis examines axial concentration profiles of the lean solids phase and the corresponding evolution of mixing from the onset to steady state. To characterize this transition quantitatively, characteristic mixing lengths and timescales are determined, and the corresponding transitional mixing velocities are calculated. These assessments are further supported by a frequency-based analysis of fluctuations in both pressure and lean solids concentration, as well as by a mixing index, which provides a measure of the quality of the established mixing under the different operating conditions.

4.3.1 Transient Mixing

Table 4.1 summarizes the penetration lengths and characteristic mixing times observed at the onset of mixing, following the fate of lean solids that first rest at the bed surface, then populate other heights after the abrupt increase in fluidization velocity from minimum fluidization to the operating condition. The penetration length represents the characteristic depth reached by the lean solids phase during this initial transient, while the mixing time defines the timescale required for the lean solids to reach this depth and for the system to transition away from the initially segregated state.

The measurements show that both penetration length and mixing time increase with bed height and fluidization velocity, reflecting enhanced axial transport and solids circulation at the onset of mixing for H_{bed} > 0.3m. In contrast, shallow beds (H_{bed} = 0.15m) exhibit constrained penetration of lean solids, which appear largely confined to the bed surface, even at higher fluidization velocities. This behavior is attributed to the limited bed height and weaker axial circulation of bulk solids. In such shallow beds, bubbles do not fully develop and have short residence times, allowing gas to escape rapidly without entraining lean solids in the bubble wake or inducing particle splashing. These observations highlight bed height as a key threshold parameter governing the onset of mixing.

Further, the penetration length of lean solids remains independent of loading up to a critical value and generally increases with fluidization velocity. Beyond a critical lean solids loading of approximately 10 %$_{vol}$, the lean phase accumulates near the bed surface, forming a thick surface layer that inhibits bubble eruption during the abrupt modification of the velocity. Instead, bubbles tend to split or percolate through this layer, which reduces the downward transport of lean solids and limits overall axial circulation of bulk solids. As a result, the characteristic penetration length decreases, indicating that higher fluidization velocities or additional operational adjustments are required to establish mixing.

Table 4.2: Characteristic scales for the onset of mixing in the lean solids phase. Source: Paper II

Conc. of lean solids phase ($\varkappa_{lean}$) [$\%_{Vol}$]	Aspect ratio (H/D) [-]	Bed height (H_{bed}) [m]	Characteristic Scales	Fluidization Number $\left(\frac{u_0}{u_{mf}}\right)$ [-]					
				1.5	2	2.5	3	3.5	4
3	0.27	0.3	L* [m]	0.058	0.115	0.115	0.192	0.192	0.288
			τ_{mix}* [s]	12.98 ± 1.6	11.91 ± 2.6	10.47 ± 1.18	13.71 ± 1.7	13.64 ± 0.69	16.67 ± 0.58
5	0.27	0.3	L* [m]	0.058	0.115	0.115	0.192	0.192	0.288
			τ_{mix}* [s]	13.92 ± 2.53	11.88 ± 1.54	11.03 ± 0.67	18.07 ± 4.78	13.08 ± 0.46	16.53 ± 1.42
10	0.13	0.15	L* [m]	0.038	0.077	0.077	0.077	0.077	0.077
			τ_{mix}* [s]	14.04 ± 1.92	18.50 ± 2.04	17.23 ± 1.83	16.7 ± 4.31	15.8 ± 1.83	14.85 ± 0.43
	0.27	0.3	L* [m]	0.058	0.115	0.192	0.192	0.192	0.288
			τ_{mix}* [s]	14.49 ± 2.59	10.84 ± 0.61	18.26 ± 3.77	13.92 ± 3.29	13.31 ± 2.03	18.13 ± 4.45
	0.4	0.46	L* [m]	0.115	0.115	0.192	0.25	0.31	0.385
			τ_{mix}* [s]	14 ± 0.44	11.11 ± 1.37	15.32 ± 2.76	13.71 ± 2.04	11.91 ± 1.93	13.89 ± 2.10
20	0.27	0.3	L* [m]	0.058	0.058	0.115	0.115	0.192	0.192
			τ_{mix}* [s]	16.65 ± 5.62	11.47 ± 1.01	12.98 ± 0.28	13.17 ± 2.77	14.88 ± 1.97	13.95 ± 1.70

Figure 4.7 graphically shows the evolution of penetration lengths and their corresponding mixing timescales for the selected case of a bed height of H_{bed} = 0.3m, and a lean solids loading of $\varkappa_{lean}$ = 10 $\%_{vol}$, (fourth row in **Table 4.1**). The figure shows that at the onset of mixing, increasing fluidization velocity leads, in general, to deeper penetration of the lean solids into the dense bed and, consequently, to longer times required for the lean solids to travel from the bed surface to the attained depth. However, this trend is not monotonic. Beyond a certain velocity, the characteristic time required to reach a given depth decreases, reflecting enhanced solids mobility and stronger convective transport.

It must be noted that the characteristic lengths are assessed based on the axial position of the coils in the pin, and therefore, the characteristic length (L^*) can only take specific discrete values. A fully resolved length scale would show more accurately the interplay between characteristic lengths and times.

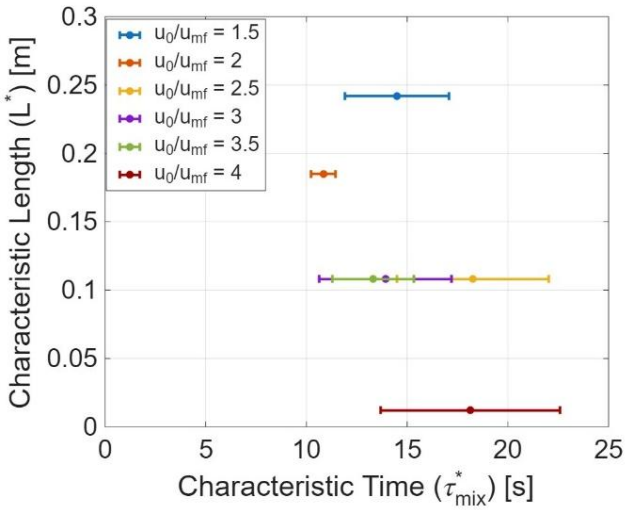

Figure 4.7: Penetration depth as a function of time. Conditions: H_{bed} = 0.3m, and $\varkappa_{lean}$ = 10$\%_{vol}$.

The characteristic mixing lengths and times provide also a quantitative basis for defining transitional fluidization velocities, i.e., the velocities at which the lean solids phase transitions from a segregated to a mixed state.

Figure 4.8 presents the transitional mixing velocities for the range of bed heights investigated. In general, increasing fluidization velocity accelerates the transition from a segregated to a mixed state, leading to higher transitional velocities. Bed height plays a key role in modulating this behavior: taller beds exhibit higher transitional velocities, as the increased axial extent allows bubbles to grow, coalesce, and persist over longer rise distances. This enhanced bubble development strengthens solids circulation and extends the effective mixing length required for the lean solids to penetrate the dense bed during the transition.

In contrast, shallow beds reach a mixed state at lower transitional velocities. Although lean solids penetrate to shallower depths, bubble growth is limited by the reduced bed height, resulting in shorter bubble residence times and weaker circulation. Under these conditions, the characteristic mixing times remain comparable to those of taller beds, despite the reduced penetration depth.

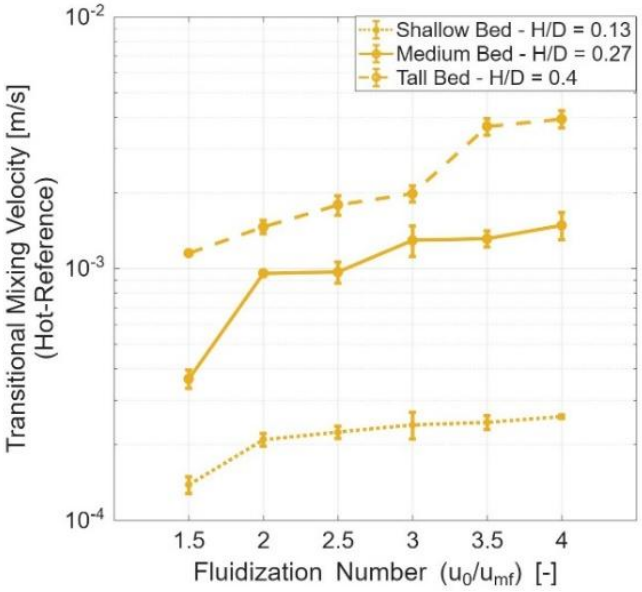

Figure 4.8: Transitional mixing velocities as a function of fluidization velocity across varying bed height. Conditions: $\varkappa_{lean}$ = 10%vol. Source: Paper II

The effect of lean solids loading is found to be negligible within the range studied and is therefore not discussed here; corresponding results are provided in appended **Paper II** (refer to Figure 11).

4.3.2 Steady-State Mixing

Figure 4.9 compiles the mixing index values (**Eq. 2.6**) obtained over the range of operating conditions examined in experimental **Campaign II**. In all bed configurations and for varying lean solids loadings, higher fluidization velocities consistently yield larger mixing indices, reflecting improved axial mixing of the lean solids phase. This trend is in good agreement with previous studies [13,28,82,88–90] and is generally attributed to more vigorous bubble activity: elevated fluidization velocities generate larger, faster-rising bubbles that enhance solids transport [91].

The influence of lean solids loading is illustrated in **Figure 4.9a**. For volumetric loadings up to 10%$_{vol}$, the mixing index is relatively insensitive to changes in loading at a given fluidization velocity. At 20%$_{vol}$, however, mixing performance declines markedly. Under these conditions, a substantial accumulation of lean solids forms near the bed surface, creating a thick surface layer that alters fluidization dynamics. Bubble eruptions at the surface are suppressed, forcing bubbles to split and percolate through the layer rather than promoting effective solids circulation. This reduces both upward and downward transport, weakening axial mixing and lowering the overall mixing index. Increasing fluidization velocity partially mitigates this effect, but a significant fraction of the lean solids remains confined to the surface, limiting penetration into the dense bed. For loadings below this critical threshold (≤10%$_{vol}$), the mixing index approaches an asymptotic value of approximately 0.7–0.8 for fluidization numbers $u_0/u_{mf} \approx 3$.

Figure 4.9b examines the effect of bed height at a constant lean solid loading of 10%$_{vol}$. The shallow bed exhibits weak mixing, with only marginal improvements as fluidization velocity increases. Medium and tall beds, however, display nearly identical mixing indices across the same velocity range. This indicates that, once a minimum bed aspect ratio—here H/D ≈ 0.27—is exceeded, axial mixing of the lean solids phase becomes largely independent of bed height.

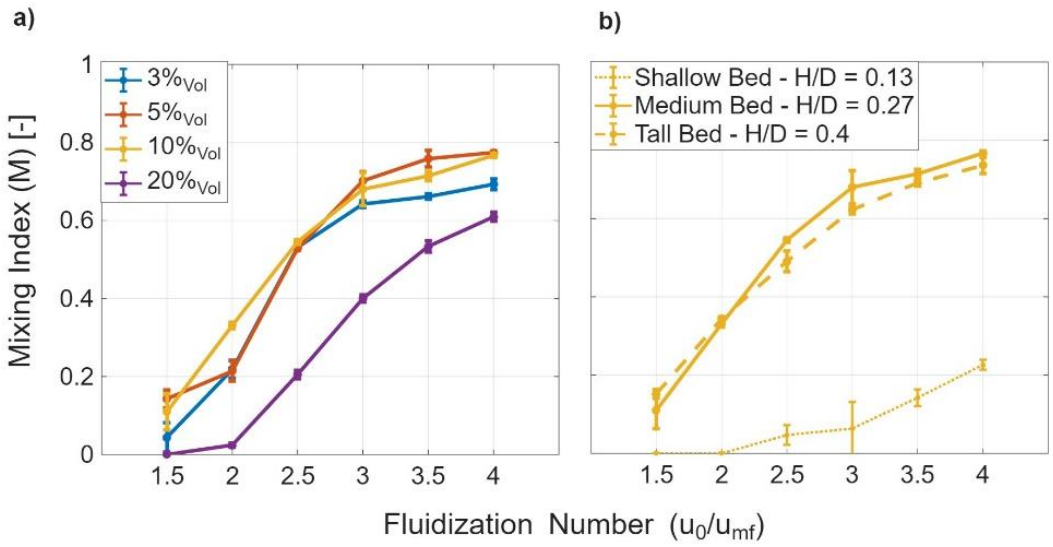

Figure 4.9: Mixing index dependency on the fluidization velocity. (a) Varying lean solids phase loading for H/D = 0.27, (b) Varying bed height at constant volumetric loading of the lean solids phase, $\varkappa_{lean}$ = 10%$_{vol}$.
Source: Paper II

Figure 4.10 shows the cumulative frequency spectra of pressure and lean solids concentration fluctuations for different bed heights, enabling a direct comparison between overall bed hydrodynamics and mixing-relevant solids motion. Pressure fluctuations characterize the dominant bed dynamics and are associated primarily with bubble formation, growth, and eruption. The spectra show median frequencies (f_{50}) below approximately 6 Hz in the shallow bed and below 3 Hz in the medium bed, with only a marginal shift as bed height increases.

In contrast, fluctuations in lean solids concentration are dominated by significantly lower frequencies, with median frequency (f_{50}) below 1 Hz, indicating that effective transport and redistribution of lean solids occur on much longer timescales than the dominant bubble activity. Although the shallow bed exhibits more frequent pressure fluctuations, consistent with intensified bubbling, this increase is not reflected in the concentration spectra, which remain largely insensitive to bed height.

This disparity demonstrates that the majority of bubble-related events do not lead to measurable transport of lean solids. Only a limited subset of bubble interactions—likely those involving sufficiently large or coherent structures that induce sustained solids circulation—contributes to effective mixing. Based on the ratio between characteristic pressure and concentration fluctuation frequencies, it is inferred that in the shallow bed, approximately one-sixth of the bubble events contribute to lean solids mixing, whereas in the medium and tall beds, this fraction increases to roughly one-third, reflecting the enhanced effectiveness of bubble-induced circulation with increasing bed height.

Since the frequency analysis shows minimal dependence on fluidization velocity and lean solids loading, further result data on this impact are omitted here but can be found in the appended **Paper II** (Figure 10).

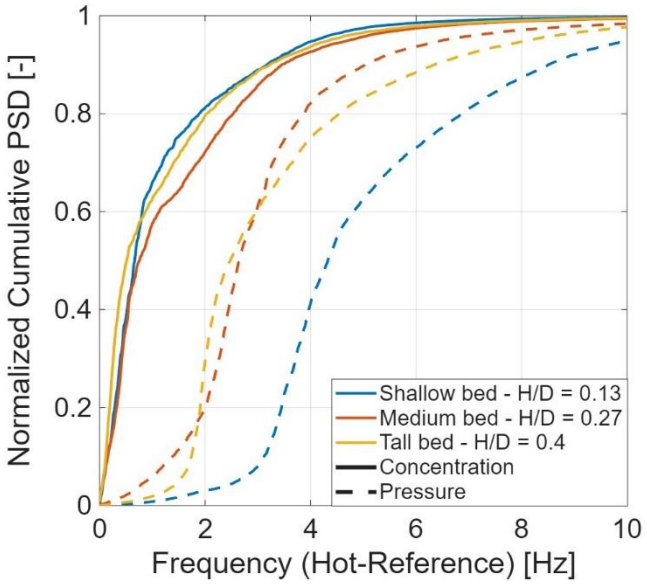

Figure 4.10: Cumulative power spectra of the time series of the pressure (dashed line) and lean solids phase concentration (solid line) for varying bed height. Source: Paper II

4.4 Significance of gas release on Mixing Behavior

The preceding sections established the baseline mixing behavior of larger and lighter particles in the absence of gas release. Building on this, the present section summarizes the results from experimental **Campaign III**, examining how particle gas release alters mixing by introducing a localized gas source and influencing both axial and lateral transport across varying fluidization velocities and lean solids. The gas release conditions mimicked in this campaign represent scenarios relevant to biomass drying and devolatilization. Details of the imposed gas release rates are provided in the appended **Paper III** (see Section 2 and Figure 2).

To isolate the effects of particle size and density under gas-releasing conditions, three types of lean solids tracers were investigated at four fluidization velocities (see Table 2 in appended **Paper III** for details):

- ***Reference tracer***: baseline case, representative of the lean solids (≈70 mm, 550 kg/m³), used to capture the mixing behavior of a biomass pellet. Inherently buoyant relative to the surrounding solids suspension.
- ***Larger tracer***: increased size (≈115 mm) but similar density to the reference, to examine the effect of particle size. Inherently buoyant relative to the surrounding solids suspension.
- ***Heavier tracer***: similar in size to the reference (≈67 mm) but with a higher density (≈1500 kg/m³), to evaluate the effect of particle density on transport. Non-buoyant relative to the surrounding solids suspension.
- ***Blank controls***: identical in size and density to the gas-releasing tracers but without gas release, used to isolate the influence of gas on mixing behavior.

4.4.1 Axial Mixing

Figure 4.11 shows the axial distributions of gas-releasing and blank (non-releasing) lean solids particles for the three types across four fluidization velocities. Similar to the blank tracer case and consistent with their intrinsic properties, the gas-releasing reference and larger particles predominantly remain near the bed surface, whereas the heavier particle is the only one showing a significant influence of the gas release on its mixing, as for moderate fluidization velocities, it immerses to a larger extent into the dense bed. Increasing fluidization velocity generally shifts all distributions upward, most noticeably for the reference particle, due to bed expansion, and broadens the distributions, reflecting enhanced axial mixing.

The effect of gas release strongly depends on the particle's inherent tendency to segregate. For reference and larger particles, which are intrinsically buoyant, gas release has only a minor influence. At low velocities ($u_0/u_{mf} \leq 2$), gas-releasing particles penetrate slightly deeper, but this effect diminishes at higher velocities. In contrast, the heavier particles are more strongly affected. At low velocities, gas release promotes upward displacement toward the bed surface, with this effect persisting until $u_0/u_{mf} \approx 3.5$. At higher velocities, the influence weakens and disappears by $u_0/u_{mf} = 5$, where releasing and non-releasing heavier particles exhibit identical distributions.

Gas release can, in principle, render heavier non-buoyant particles effectively buoyant while further enhancing the buoyancy of already buoyant particles when immersed in the dense bed [58]. The present results, however, reveal a different mechanism when fed to the bed surface. Sideways gas release from the particles locally displaces the bulk solids beneath them, causing the particles to sink deeper into the bed. At low fluidization velocities, the gas–solid flow is insufficient to refill the void created by the released gas, leading to net downward motion of the particles. This behavior contrasts with previous reports for fully immersed particles. At higher fluidization velocities, strong convective flows around

the gas-releasing particles rapidly sweep away the released gas, thereby diminishing the influence of gas release and causing the particles to behave similarly to blank particles.

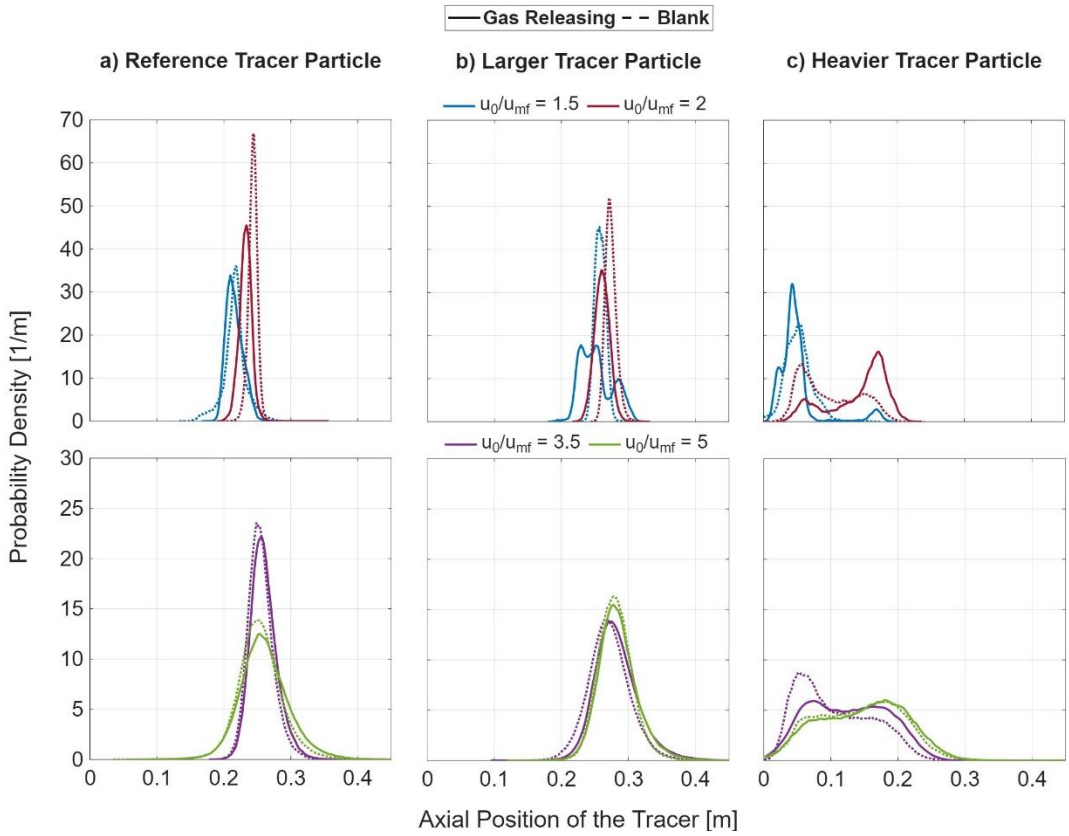

Figure 4.11: Probability density function of the axial location of the gas-releasing lean solid for different fluidization velocities (u_0/u_{mf} = 1.5 and 2 in the top row, and u_0/u_{mf} = 3.5 and 5 in the bottom row); a) Reference tracer; b) Larger tracer; and c) Heavier tracer. Source: Paper III

4.4.2 Lateral Mixing

The lateral mixing of the lean solids was quantified through their lateral dispersion coefficients using **Eq 2.7** and is presented in **Figure 4.12** for the four fluidization velocities tested. For all types of particles, the lateral dispersion coefficient increases with fluidization velocity for both blank (non-releasing) and gas-releasing lean solids, consistent with previous observations [92].

Overall, blank and gas-releasing particles exhibit coefficients of the same order of magnitude. Gas release, however, typically enhances lateral dispersion by 30–40%. Exceptions occur for the larger particles at u_0/u_{mf} = 5 and the heavier particles at u_0/u_{mf} = 2, where the dispersion coefficients of blank and gas-releasing particles are nearly identical or slightly higher for the blank particle.

Interestingly, while axial motion becomes largely unaffected by gas release at higher fluidization velocities (i.e., $u_0/u_{mf} \geq 3.5$), lateral movement remains strongly influenced. This behavior can be attributed to the asymmetric gas release flux, which imparts repeated small horizontal impulses to the particle in different directions [93]. Consequently, when axial motion is weakly affected by gas release, lateral dispersion is enhanced; conversely, when axial transport dominates, lateral spreading is minimal.

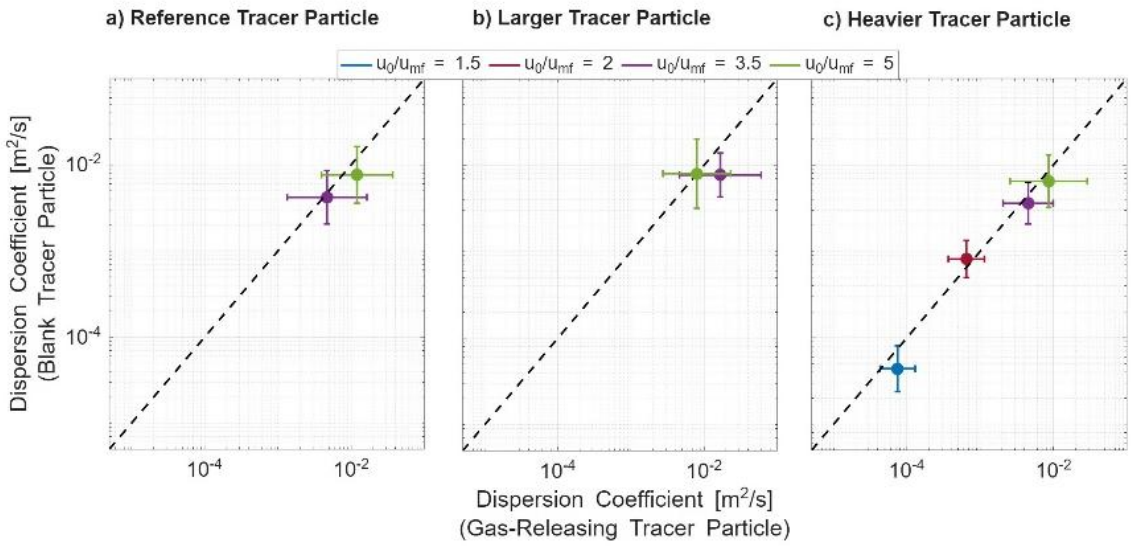

Figure 4.12: Lateral dispersion coefficients of gas-releasing and non-releasing lean solid particles at different fluidization velocities. Source: Paper III

5 Conclusions

This thesis demonstrates the capability of a newly developed implementation of the magnetic solids tracing technique, featuring a pin-probe configuration, to resolve spatiotemporal distributions and dynamics of solids in fluidized beds. By enabling space- and time-resolved quantification of axial solids mixing, this technique provides direct insights into mixing dynamics and their dependence on operating conditions in binary fluidized systems.

A central conclusion is that scaling matters: cold-unscaled laboratory experiments do not faithfully reproduce the hydrodynamics of industrial hot beds. The observed overestimation of bubble sizes and solids redistribution at intermediate and higher fluidization velocities, and the overprediction of segregation at low velocities, illustrate that unscaled tests can misrepresent key mixing mechanisms. Properly scaled experiments are therefore essential for ensuring that laboratory insights are transferable to industrial applications, particularly when designing or optimizing fluidized bed reactors.

The governing factors controlling axial mixing were systematically investigated through variation of fluidization velocity, bed height, and lean solids loading under fluid-dynamically scaled conditions. Increasing fluidization velocity and bed height enhances lean solids circulation and axial mixing by strengthening convective transport within the bulk solids. In contrast, increasing lean solids loading suppresses bubble-driven circulation; when the lean solids volume fraction exceeds a critical threshold of approximately 10 $\%_{vol}$, mixing deteriorates due to the formation of a persistent surface layer. These results indicate that operating conditions can be strategically tuned to achieve desired mixing characteristics and that exceeding certain solids loadings may negatively impact reactor performance. Consequently, controlled mixing or segregation can be established by manipulating these key parameters. Characteristic penetration lengths and mixing times provide a robust framework for defining transitional mixing velocities, which increase with bed height and fluidization velocity, reflecting the rapid onset of established mixing.

Lastly, particle-centric gas release was shown to introduce additional transport mechanisms that can significantly modify solids mixing for specific cases. At low fluidization velocities, gas release restricts axial particle motion and promotes segregation, an effect most pronounced for heavier particles, while lighter particles remain largely unaffected. At higher velocities, its influence shifts toward enhanced lateral dispersion, resulting in increased lateral mixing. Neglecting these gas-release effects, particularly the impact on lateral transport, can therefore lead to underestimation of particle residence times and misrepresentation of solids transport pathways, with potentially significant consequences for reactor performance and conversion efficiency.

Collectively, these findings establish a robust framework for interpreting binary solids mixing in fluidized beds, providing both methodological validation and fundamental insight. The results underscore the need for carefully designed experiments and scaling considerations to predict industrial-scale behavior, while offering quantitative metrics—penetration lengths, mixing times, and transitional velocities, lateral dispersion coefficients for gas-releasing particles—that can guide the optimization of reactor design and operation. Overall, this work advances both experimental methodology and fundamental understanding of mixing in binary fluidized beds and provides a validated framework for interpreting cold experiments in the context of industrial hot fluidized-bed processes.

6 Future work

Building on the findings of the parametric studies presented in this thesis, a promising direction for future research is the intentional exploitation of controlled segregation to operate fluidized beds as continuous separation devices, with relevance to the continuous production of biochar. Rather than mitigating segregation, this approach seeks to harness predictable particle stratification to achieve solids product separation. The parameters identified in this work suggest that segregation can be promoted under relatively low fluidization velocities, higher lean solids fractions, and reduced bed aspect ratios, providing a foundation for future implementation of controlled separation strategies.

Future work ought to investigate segregation behavior in a bubbling fluidized bed with an imposed solid crossflow, enabling continuous feeding and separation of solids. Such a configuration would allow systematic evaluation of separation yields of the lean solids phase (biochar) under varying operating conditions, providing quantitative performance metrics for segregation-based separation.

In addition, detailed analysis of the residence time distribution of the lean solids phase can offer insights into transport pathways and timescales governing both segregation and separation. Understanding these dynamics is essential for designing separators that balance separation efficiency with throughput and operational stability.

To support process design and scale-up, future studies aim to develop and further validate a mechanistic model describing the segregation and separation behavior of the lean solids phase. Such a model can link particle properties, bed hydrodynamics, and solids crossflow, enabling predictive assessment of fluidized bed separators and facilitating their integration into continuous biochar production systems.

Nomenclature

Symbols

D_b	Diameter of the bubble	[m]
D_{lean}	Dispersion coefficient of lean solids	[m^2/s]
d_p	Diameter of particle	[mm]
FN	Fluidization number	[-]
f	Frequency	[Hz]
g	Gravitational constant, 9.81	[m/s^2]
Δh	Height interval	[m]
H_{bed}	Static bed height	[m]
L	Length	[m]
L*	Characteristic length	[m]
M	Mixing Index	[-]
P	Pressure	[Pa]
ΔP	Pressure drop	[Pa]
Δt	Time interval	[s]
T	Temperature	[°C]
τ_{mix}*	Characteristic time of mixing	[s]
τ_{seg}*	Characteristic time of segregation	[s]
u_0	Fluidization velocity	[m/s]
u_{mf}	Minimum fluidization velocity	[m/s]
Δ_{xy}	Threshold length in x-y plane	[m]
ε_g	Bed voidage	[-]
ε_s	Volumetric concentration of solids	[-]
Φ	Sphericity	[-]
σ	Standard Deviation	[-]
$\varkappa$	Loading of the solids phase	[$\%_{vol}$]
ρ	Density	[kg/m^3]
μ	Viscosity	[N/m.s}

Subscripts

bulk	Bulk solids phase
g	Gas phase
lean	Lean solids phase
s	Solids

References

[1] D. Kunii, O. Levenspiel, Industrial Applications of Fluidized Beds, in: Fluid. Eng., Elsevier, 1991: pp. 15–59. https://doi.org/10.1016/B978-0-08-050664-7.50008-1.

[2] J.R. Grace, X. Bi, N. Ellis, Essentials of fluidization technology, 2020. https://doi.org/10.1002/9783527699483.

[3] F. Winter, B. Schratzer, Applications of fluidized bed technology in processes other than combustion and gasification, in: Fluid. Bed Technol. Near-Zero Emiss. Combust. Gasif., Elsevier, 2013: pp. 1005–1033. https://doi.org/10.1533/9780857098801.5.1005.

[4] O. Dogu, M. Pelucchi, R. Van de Vijver, P.H.M. Van Steenberge, D.R. D'hooge, A. Cuoci, M. Mehl, A. Frassoldati, T. Faravelli, K.M. Van Geem, The chemistry of chemical recycling of solid plastic waste via pyrolysis and gasification: State-of-the-art, challenges, and future directions, Prog. Energy Combust. Sci. 84 (2021) 100901. https://doi.org/10.1016/j.pecs.2020.100901.

[5] J. Li, L. Wen, G. Qian, H. Cui, M. Kwauk, J.C. Schouten, C.M. Van den Bleek, Structure heterogeneity, regime multiplicity and nonlinear behavior in particle-fluid systems, Chem. Eng. Sci. 51 (1996) 2693–2698. https://doi.org/10.1016/0009-2509(96)00138-8.

[6] J.F. Davidson, R. Clift, D. Harrison, Fluidization, Academic Press, 1985. https://books.google.se/books?id=W79TAAAAMAAJ.

[7] M. Wirsum, F. Fett, N. Iwanowa, G. LGBRjanow, Particle mixing in bubbling fluidized beds of binary particle systems, Powder Technol. 120 (2001) 63–69. https://doi.org/10.1016/S0032-5910(01)00348-5.

[8] G. Olivieri, A. Marzocchella, P. Salatino, Segregation of fluidized binary mixtures of granular solids, AIChE J. 50 (2004) 3095–3106. https://doi.org/10.1002/aic.10340.

[9] O.O. Olaofe, K.A. Buist, N.G. Deen, M.A. van der Hoef, J.A.M. Kuipers, Segregation dynamics in dense polydisperse gas-fluidized beds, Powder Technol. 246 (2013) 695–706. https://doi.org/10.1016/j.powtec.2013.05.047.

[10] B. Cluet, G. Mauviel, Y. Rogaume, O. Authier, A. Delebarre, Segregation of wood particles in a bubbling fluidized bed, Fuel Process. Technol. 133 (2015) 80–88. https://doi.org/10.1016/j.fuproc.2014.12.045.

[11] P. Brachi, R. Chirone, F. Miccio, M. Miccio, G. Ruoppolo, Segregation and fluidization behavior of poly-disperse mixtures of biomass and inert particles, Chem. Eng. Trans. 57 (2017) 811–816. https://doi.org/10.3303/CET1757136.

[12] L. Molignano, M. Troiano, R. Solimene, S. Tebianian, J.-F. Joly, P. Salatino, Investigation of mixing/segregation patterns of two dissimilar granular solids in fluidized beds by capacitance probes, Chem. Eng. Sci. 322 (2026) 123047. https://doi.org/10.1016/j.ces.2025.123047.

[13] S.Y. Wu, J. Baeyens, Segregation by size difference in gas fluidized beds, Powder Technol. 98 (1998) 139–150. https://doi.org/10.1016/S0032-5910(98)00026-6.

[14] W.R.A. Goossens, Classification of fluidized particles by archimedes number, Powder Technol. 98 (1998) 48–53. https://doi.org/10.1016/S0032-5910(98)00027-8.

[15] G.–. Yang, D.–. Zheng, J.–. Zhou, Y.–. Zhao, Q.–. Chen, Air classification of moist raw coal in a vibrated fluidized bed, Miner. Eng. 15 (2002) 623–625. https://doi.org/10.1016/S0892-6875(02)00057-2.

[16] J.L. -P. Chen, D.L. Keairns, Particle segregation in a fluidized bed, Can. J. Chem. Eng. 53 (1975) 395–402. https://doi.org/10.1002/cjce.5450530407.

[17] M. Miccio, P. Brachi, G. Ruoppolo, F. Miccio, R. Chirone, B. Tauleigne, Fluidized Bed Design and Process Calculations for the Continuous Torrefaction of Tomato Peels with Solid Product

Separation, Chem. Eng. Trans. 99 (2023) 49–54. https://doi.org/10.3303/CET2399009.

[18] T. Berdugo Vilches, H. Thunman, Experimental Investigation of Volatiles-Bed Contact in a 2-4 MWth Bubbling Bed Reactor of a Dual Fluidized Bed Gasifier, Energy and Fuels 29 (2015) 6456–6464. https://doi.org/10.1021/acs.energyfuels.5b01303.

[19] E. Sette, T. Berdugo Vilches, D. Pallarès, F. Johnsson, Measuring fuel mixing under industrial fluidized-bed conditions - A camera-probe based fuel tracking system, Appl. Energy 163 (2016) 304–312. https://doi.org/10.1016/j.apenergy.2015.11.024.

[20] V. Del Duca, P. Brachi, R. Chirone, R. Chirone, A. Coppola, M. Miccio, G. Ruoppolo, Binary mixtures of biomass and inert components in fluidized beds: Experimental and neural network exploration, Fuel 346 (2023) 128314. https://doi.org/10.1016/j.fuel.2023.128314.

[21] S. Parvathaneni, V. V. Buwa, Role of bubbling behaviour in segregation and mixing of binary gas-solids flow of particles with different density, Powder Technol. 372 (2020) 178–191. https://doi.org/10.1016/j.powtec.2020.05.072.

[22] Y. Li, L. Du, Y. Zhao, Z. Wang, F. Zhu, Z. Lu, C. Duan, L. Dong, C. Zhou, Segregation and mixing behavior of geldart D binary particles in pulsed gas-solid fluidized bed, Part. Sci. Technol. 40 (2022) 434–444. https://doi.org/10.1080/02726351.2021.1954116.

[23] H.T. Jang, T.S. Park, W.S. Cha, Mixing-segregation phenomena of binary system in a fluidized bed, J. Ind. Eng. Chem. 16 (2010) 390–394. https://doi.org/10.1016/j.jiec.2009.10.003.

[24] K.V.N.S. Rao, G. V. Reddy, Cold flow studies of rice husk, saw dust, and groundnut shell fuels in a fluidized bed, Energy Sources, Part A Recover. Util. Environ. Eff. 32 (2010) 1701–1711. https://doi.org/10.1080/15567030902882893.

[25] K. Zhang, B. Yu, J. Chang, G. Wu, T. Wang, D. Wen, Hydrodynamics of a fluidized bed co-combustor for tobacco waste and coal, Bioresour. Technol. 119 (2012) 339–348. https://doi.org/10.1016/j.biortech.2012.05.132.

[26] F. Fotovat, R. Ansart, M. Hemati, O. Simonin, J. Chaouki, Sand-assisted fluidization of large cylindrical and spherical biomass particles: Experiments and simulation, Chem. Eng. Sci. 126 (2015) 543–559. https://doi.org/10.1016/j.ces.2014.12.022.

[27] T. Emiola-Sadiq, J. Wang, L. Zhang, A. Dalai, Mixing and segregation of binary mixtures of biomass and silica sand in a fluidized bed, Particuology 58 (2021) 58–73. https://doi.org/10.1016/j.partic.2021.01.010.

[28] Y. Zhang, B. Jin, W. Zhong, Experimental investigation on mixing and segregation behavior of biomass particle in fluidized bed, Chem. Eng. Process. Process Intensif. 48 (2009) 745–754. https://doi.org/10.1016/j.cep.2008.09.004.

[29] R.K. Upadhyay, S. Roy, Investigation of hydrodynamics of binary fluidized beds via radioactive particle tracking and dual-source densitometry, Can. J. Chem. Eng. 88 (2010) 601–610. https://doi.org/10.1002/cjce.20334.

[30] L. Kalo, H.J. Pant, M.C. Cassanello, R.K. Upadhyay, Time series analysis of a binary gas-solid conical fluidized bed using radioactive particle tracking (RPT) technique data, Chem. Eng. J. 377 (2019) 119807. https://doi.org/10.1016/j.cej.2018.08.193.

[31] A. Köhler, D. Pallarès, F. Johnsson, Magnetic tracking of a fuel particle in a fluid-dynamically down-scaled fluidised bed, Fuel Process. Technol. 162 (2017) 147–156. https://doi.org/10.1016/j.fuproc.2017.03.018.

[32] A. Köhler, A. Rasch, D. Pallarès, F. Johnsson, Experimental characterization of axial fuel mixing in fluidized beds by magnetic particle tracking, Powder Technol. 316 (2017) 492–499. https://doi.org/10.1016/j.powtec.2016.12.093.

[33] E. Sette, D. Pallarès, F. Johnsson, F. Ahrentorp, A. Ericsson, C. Johansson, Magnetic tracer-particle tracking in a fluid dynamically down-scaled bubbling fluidized bed, Fuel Process.

Technol. 138 (2015) 368–377. https://doi.org/10.1016/j.fuproc.2015.06.016.

[34] D. Werner, H. Davison, E. Robinson, J.A. Sykes, J.P.K. Seville, A. Wellings, S. Bhattacharya, D.A. Sanchez Monsalve, T. Kokalova Wheldon, C.R.K. Windows-Yule, Effect of system composition on mixing in binary fluidised beds, Chem. Eng. Sci. 271 (2023) 118562. https://doi.org/10.1016/j.ces.2023.118562.

[35] D. Bellgardt, J. Werther, A novel method for the investigation of particle mixing in gas-solid systems, Powder Technol. 48 (1986) 173–180. https://doi.org/10.1016/0032-5910(86)80076-6.

[36] M.J. Rhodes, S. Zhou, T. Hirama, H. Cheng, Effects of operating conditions on longitudinal solids mixing in a circulating fluidized bed riser, AIChE J. 37 (1991) 1450–1458. https://doi.org/10.1002/aic.690371003.

[37] J.A. Valenzuela, L.R. Glicksman, An experimental study of solids mixing in a freely bubbling two-dimensional fluidized bed, Powder Technol. 38 (1984) 63–72. https://doi.org/10.1016/0032-5910(84)80034-0.

[38] D. Liu, X. Chen, Quantifying lateral solids mixing in a fluidized bed by modeling the thermal tracing method, AIChE J. 58 (2012) 745–755. https://doi.org/10.1002/aic.12627.

[39] A.T. Harris, J.F. Davidson, R.B. Thorpe, Particle residence time distributions in circulating fluidised beds, Chem. Eng. Sci. 58 (2003) 2181–2202. https://doi.org/10.1016/S0009-2509(03)00082-4.

[40] C. Yan, Y. Fan, C. Lu, Y. Zhang, Y. Liu, R. Cao, J. Gao, C. Xu, Solids mixing in a fluidized bed riser, Powder Technol. 193 (2009) 110–119. https://doi.org/10.1016/j.powtec.2009.02.015.

[41] L. Weigang, C.E. Weinell, P.F.B. Hansen, K. Dam-Johansen, Hydrodynamics of a commercial scale CFB boiler-study with radioactive tracer particles, Chem. Eng. Sci. 54 (1999) 5495–5506. https://doi.org/10.1016/s0009-2509(99)00296-1.

[42] D.C. Guío-Pérez, T. Pröll, J. Wassermann, H. Hofbauer, Design of an inductance measurement system for determination of particle residence time in a dual circulating fluidized bed cold flow model, Ind. Eng. Chem. Res. 52 (2013) 10732–10740. https://doi.org/10.1021/ie400211h.

[43] D.C. Guío-Pérez, T. Pröll, H. Hofbauer, Measurement of ferromagnetic particle concentration for characterization of fluidized bed fluid-dynamics, Powder Technol. 239 (2013) 147–154. https://doi.org/10.1016/j.powtec.2013.01.040.

[44] D.C. Guío-Pérez, F. Dietrich, J.N. Ferreira Cala, T. Pröll, H. Hofbauer, Estimation of solids circulation rate through magnetic tracer tests, Powder Technol. 316 (2017) 650–657. https://doi.org/10.1016/j.powtec.2017.04.062.

[45] M. Farha, D.C. Guío-Pérez, F. Johnsson, D. Pallarès, Characterization of the solids crossflow in a bubbling fluidized bed, Powder Technol. 443 (2024). https://doi.org/10.1016/j.powtec.2024.119967.

[46] N. Nemati, T. Pröll, T. Mattisson, M. Rydén, Impact of random packing on residence time distribution of particles in bubbling fluidized beds: Part 1–cross-current flow reactors, Chem. Eng. Sci. 302 (2025). https://doi.org/10.1016/j.ces.2024.120724.

[47] N. Nemati, T. Mattisson, D. Pallarès, D.C. Guío-Pérez, M. Rydén, Impact of random packing on residence time distribution of particles in bubbling fluidized beds: Part 2 - Counter-current flow reactors, Powder Technol. 465 (2025). https://doi.org/10.1016/j.powtec.2025.121306.

[48] A. Gómez-Barea, B. Leckner, Modeling of biomass gasification in fluidized bed, Prog. Energy Combust. Sci. 36 (2010) 444–509. https://doi.org/10.1016/j.pecs.2009.12.002.

[49] M.S. Alagha, P. Szentannai, A conservative macroscopic model for binary-mixture fluidized beds, Period. Polytech. Chem. Eng. 65 (2021) 525–535. https://doi.org/10.3311/PPch.17420.

[50] A. Köhler, D.C. Guío-Pérez, A. Prati, M. Larcher, D. Pallarès, Rheological effects of a gas fluidized bed emulsion on falling and rising spheres, Powder Technol. 393 (2021) 510–518.

https://doi.org/10.1016/j.powtec.2021.07.064.

[51] A.M. Gomez, M. Nikku, P. Jalali, Direct measurement of solid drag force in fluid–particle flow, WIT Trans. Eng. Sci. 123 (2019) 11–20. https://doi.org/10.2495/MPF190021.

[52] I.N.M. Woollard, O.E. Potter, Solids mixing in fluidized beds, AIChE J. 14 (1968) 388–391. https://doi.org/10.1002/aic.690140310.

[53] J. Werther, O. Molerus, The local structure of gas fluidized beds -II. The spatial distribution of bubbles, Int. J. Multiph. Flow 1 (1973) 123–138. https://doi.org/10.1016/0301-9322(73)90008-6.

[54] H.C. Park, H.S. Choi, Influence of cross-sectional aspect ratio on biochar segregation in a bubbling fluidized bed, Sci. Rep. 12 (2022) 1–13. https://doi.org/10.1038/s41598-022-14282-y.

[55] J.G. Yates, M. MacGillivray, D.J. Cheesman, Coal devolatilisation in fluidised bed combustors, Chem. Eng. Sci. 35 (1980) 2360–2361. https://doi.org/10.1016/0009-2509(80)87019-9.

[56] M. Fiorentino, A. Marzocchella, P. Salatino, Segregation of fuel particles and volatile matter during devolatilization in a fluidized bed reactor—II. Experimental, Chem. Eng. Sci. 52 (1997) 1909–1922. https://doi.org/10.1016/S0009-2509(97)00019-5.

[57] S. Iannello, P.U. Foscolo, M. Materazzi, Investigation of single particle devolatilization in fluidized bed reactors by X-ray imaging techniques, Chem. Eng. J. 431 (2022) 133807. https://doi.org/10.1016/j.cej.2021.133807.

[58] R. Solimene, A. Marzocchella, P. Salatino, Hydrodynamic interaction between a coarse gas-emitting particle and a gas fluidized bed of finer solids, Powder Technol. 133 (2003) 79–90. https://doi.org/10.1016/S0032-5910(03)00080-9.

[59] S. Iannello, Z. Bond, A. Sebastiani, M. Errigo, M. Materazzi, Axial segregation behaviour of a reacting biomass particle in fluidized bed reactors: experimental results and model validation, Fuel 338 (2023) 127234. https://doi.org/10.1016/j.fuel.2022.127234.

[60] G. Bruni, R. Solimene, A. Marzocchella, P. Salatino, J.G. Yates, P. Lettieri, M. Fiorentino, Self-segregation of high-volatile fuel particles during devolatilization in a fluidized bed reactor, Powder Technol. 128 (2002) 11–21. https://doi.org/10.1016/S0032-5910(02)00149-3.

[61] A. Soria-Verdugo, L.M. Garcia-Gutierrez, N. García-Hernando, U. Ruiz-Rivas, Buoyancy effects on objects moving in a bubbling fluidized bed, Chem. Eng. Sci. 66 (2011) 2833–2841. https://doi.org/10.1016/j.ces.2011.03.055.

[62] D. Pallares, P.A. Díez, F. Johnsson, Experimental analysis of fuel mixing patterns in a fluidized bed, in: 12th Int. Conf. Fluid. - New Horizons Fluid. Eng., 2007. https://dc.engconfintl.org/cgi/viewcontent.cgi?article=1075&context=fluidization_xii.

[63] P.N. Rowe, B.A. Partridge, An X-ray study of bubbles in fluidised beds, Chem. Eng. Res. Des. 75 (1997) S116–S134. https://doi.org/10.1016/S0263-8762(97)80009-3.

[64] G.M. Rios, K.D. Tran, H. Masson, Free object motion in a gas fluidized bed, Chem. Eng. Commun. 47 (1986) 247–272. https://doi.org/10.1080/00986448608911767.

[65] A. Köhler, D. Pallarès, F. Johnsson, Modeling Axial Mixing of Fuel Particles in the Dense Region of a Fluidized Bed, Energy and Fuels 34 (2020) 3294–3304. https://doi.org/10.1021/acs.energyfuels.9b04194.

[66] P. Salatino, R. Solimene, Mixing and segregation in fluidized bed thermochemical conversion of biomass, Powder Technol. 316 (2017) 29–40. https://doi.org/10.1016/j.powtec.2016.11.058.

[67] H.T. Bi, A critical review of the complex pressure fluctuation phenomenon in gas–solids fluidized beds, Chem. Eng. Sci. 62 (2007) 3473–3493. https://doi.org/10.1016/j.ces.2006.12.092.

[68] F. Johnsson, R.. Zijerveld, J.. Schouten, C.. van den Bleek, B. Leckner, Characterization of

fluidization regimes by time-series analysis of pressure fluctuations, Int. J. Multiph. Flow 26 (2000) 663–715. https://doi.org/10.1016/S0301-9322(99)00028-2.

[69] J. Van Der Schaaf, J.C. Schouten, F. Johnsson, C.M. Van Den Bleek, Non-intrusive determination of bubble and slug length scales in fluidized beds by decomposition of the power spectral density of pressure time series, Int. J. Multiph. Flow 28 (2002) 865–880. https://doi.org/10.1016/S0301-9322(01)00090-8.

[70] W. Jin, J. Gao, E. Chenglin, Y. Fan, C. Lu, Pressure fluctuations in a fluidized bed of binary particles with significant differences in particle size, Chem. Eng. Sci. 287 (2024) 119704. https://doi.org/10.1016/j.ces.2024.119704.

[71] A. Einstein, Investigations on the Theory of the Brownian Movement, Courier Corporation, 1956.

[72] D.C. Guío-Pérez, F. Johnsson, D. Pallarès, Experimental investigation of the lateral mixing of large and light particles immersed in a fluidized bed, Fuel 346 (2023) 128343. https://doi.org/10.1016/j.fuel.2023.128343.

[73] L.R. Glicksman, Scaling relationships for fluidized beds, Chem. Eng. Sci. 39 (1984) 1373–1379. https://doi.org/10.1016/0009-2509(84)80070-6.

[74] M. Horio, A. Nonaka, Y. Sawa, I. Muchi, A new similarity rule for fluidized bed scale-up, AIChE J. 32 (1986) 1466–1482. https://doi.org/10.1002/aic.690320908.

[75] P.U. Foscolo, R. Di Felice, L.G. Gibilaro, L. Pistone, V. Piccolo, Scaling relationships for fluidisation: the generalised particle bed model, Chem. Eng. Sci. 45 (1990) 1647–1651. https://doi.org/10.1016/0009-2509(90)80018-A.

[76] L.R. Glicksman, M.R. Hyre, P.A. Farrell, Dynamic similarity in fluidization, Int. J. Multiph. Flow 20 (1994) 331–386. https://doi.org/10.1016/0301-9322(94)90077-9.

[77] A. Svensson, F. Johnsson, B. Leckner, Bottom bed regimes in a circulating fluidized bed boiler, Int. J. Multiph. Flow 22 (1996) 1187–1204. https://doi.org/10.1016/0301-9322(96)00025-0.

[78] J. Aronsson, A. Lyngfelt, D. Pallarès, Effects of the Choice of Gas on the Hydrodynamics of Fluidized Beds, Ind. Eng. Chem. Res. 58 (2019) 8847–8855. https://doi.org/10.1021/acs.iecr.9b00757.

[79] D.C. Guío-Pérez, F. Dietrich, J.N. Ferreira Cala, T. Pröll, H. Hofbauer, Estimation of solids circulation rate through magnetic tracer tests, Powder Technol. 316 (2017) 650–657. https://doi.org/10.1016/j.powtec.2017.04.062.

[80] M. Farha, D.C. Guío-Pérez, J. Aronsson, F. Johnsson, D. Pallarès, Assessment of experimental methods for measurements of the horizontal flow of fluidized solids under bubbling conditions, Fuel 348 (2023). https://doi.org/10.1016/j.fuel.2023.128515.

[81] A. Soria-Verdugo, L.M. Garcia-Gutierrez, S. Sanchez-Delgado, U. Ruiz-Rivas, Circulation of an object immersed in a bubbling fluidized bed, Chem. Eng. Sci. 66 (2011) 78–87. https://doi.org/10.1016/j.ces.2010.10.006.

[82] Z. Amiri, S. Movahedirad, M. Shirvani, Particles Mixing Induced by Bubbles in a Gas-Solid Fluidized Bed, 62 (2016). https://doi.org/10.1002/aic.

[83] J.P. Couderc, Incipient fluidization and particulate systems., in: J.F. Davidson, R. Clift, D. Harrison (Eds.), Fluidization, Second Edi, Academic Press, 1985: pp. 1–44.

[84] A.A. Avidan, J. Yerushalmi, Bed expansion in high velocity fluidization, Powder Technol. 32 (1982) 223–232. https://doi.org/10.1016/0032-5910(82)85024-9.

[85] F. Johnsson, S. Andersson, B. Leckner, Expansion of a freely bubbling fluidized bed, Powder Technol. 68 (1991) 117–123. https://doi.org/10.1016/0032-5910(91)80118-3.

[86] W. Jin, J. Gao, C. E, Y. Fan, C. Lu, Pressure fluctuations in a fluidized bed of binary particles

with significant differences in particle size, Chem. Eng. Sci. 287 (2024) 119704. https://doi.org/10.1016/j.ces.2024.119704.

[87] R. Jaiswal, C.E. Agu, H. Kofoed, N. Marianne, S. Eikeland, B.M.E. Moldestad, R.K. Thapa, Investigation of Bubble Properties in a Bubbling Fluidized-Bed Gasification Reactor Using a Computational Particle Fluid Dynamic Model, Ind. Eng. Chem. Res. 62 (2023) 8500–8514. https://doi.org/10.1021/acs.iecr.3c00626.

[88] N. Mostoufi, J. Chaouki, Local solid mixing in gas-solid fluidized beds, Powder Technol. 114 (2001) 23–31. https://doi.org/10.1016/S0032-5910(00)00258-8.

[89] J.F. Brainovich, MixingEegregation in Two- and Three-Dimensional Fluidized Beds : Binary Systems of Equidensity Spherical Particles, 32 (1986) 7–16.

[90] S.R. Dahl, C.M. Hrenya, Size segregation in gas – solid fluidized beds with continuous size distributions, 60 (2005) 6658–6673. https://doi.org/10.1016/j.ces.2005.05.057.

[91] D. Kunii, O. Levenspiel, Fluidization engineering, Elsevier, 2013.

[92] E. Sette, D. Pallarès, F. Johnsson, Experimental quantification of lateral mixing of fuels in fluid-dynamically down-scaled bubbling fluidized beds, Appl. Energy 136 (2014) 671–681. https://doi.org/10.1016/j.apenergy.2014.09.075.

[93] A. Elfasakhany, L. Tao, B. Espenas, J. Larfeldt, X.S. Bai, Pulverised wood combustion in a vertical furnace: Experimental and computational analyses, Appl. Energy 112 (2013) 454–464. https://doi.org/10.1016/j.apenergy.2013.04.051.